Electronic Supplementary Material (ESI) for Polymer Chemistry.

Supporting Information

The Implementation of the Catalytic Staudinger-Vilarrasa Reaction in Polymer Chemistry as a Highly Efficient Chemistry Strategy

Xiaoning Zhao,[a] Shuangshuang Zhang,[a] Tengfei Miao,[a] Shuai Li,[a] Zhengbiao Zhang,[a] Jian Zhu,[a] Wei Zhang*[a] and Xiulin Zhu[a,b]

[a]State and Local Joint Engineering Laboratory for Novel Functional Polymeric Materials, Jiangsu Key Laboratory of Advanced Functional Polymer Design and Application, Suzhou Key Laboratory of Macromolecular Design and Precision Synthesis, College of Chemistry, Chemical Engineering and Materials Science, Soochow University, Suzhou Industrial Park, Suzhou 215123, China.
[b]Global Institute of Software Technology, No 5. Qingshan Road, Suzhou National Hi-Tech District, Suzhou 215163, China

Table of Contents

Section A. Synthesis of Polyamides

1. Synthetic protocols

1) Synthesis of catalyst

Synthesis of 2,2′-dipyridyldiselenide (PySeSePy)[1]

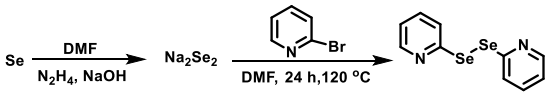

Scheme S1 Synthetic route of PySeSePy.

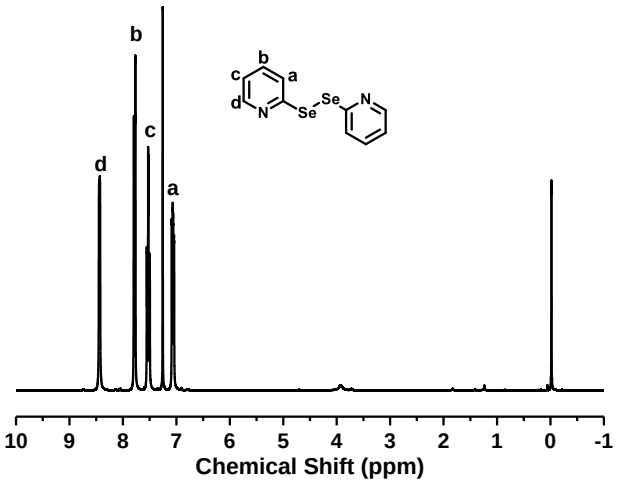

Fig. S1 ^{1}H NMR spectrum of PySeSePy at 25 °C in $CDCl_3$.

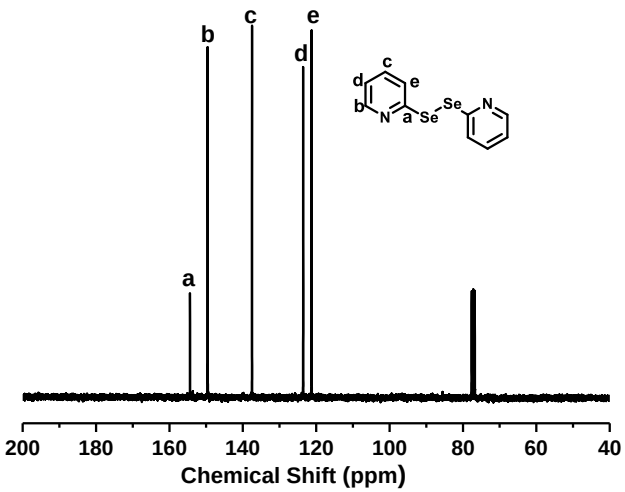

Fig. S2 ^{13}C NMR spectrum of PySeSePy at 25 °C in $CDCl_3$.

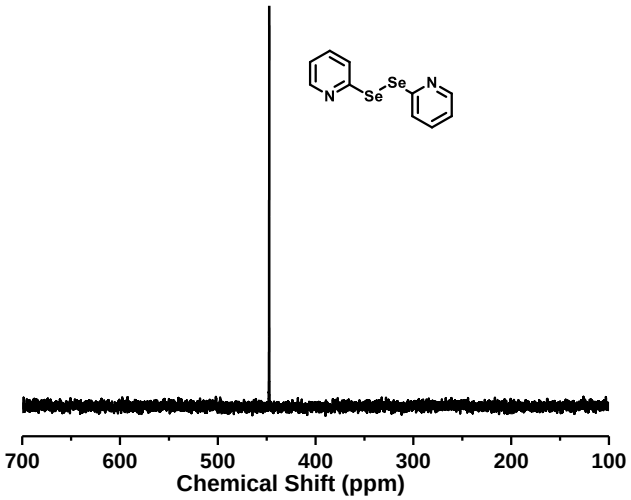

Fig. S3 ^{77}Se NMR spectrum of PySeSePy at 25 °C in $CDCl_3$.

2) Synthesis of monomers

Synthesis of 1,12-diazidododecane[2]

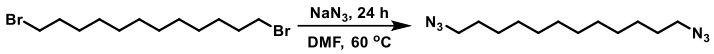

Scheme S2 Synthetic route of 1,12-diazidododecane.

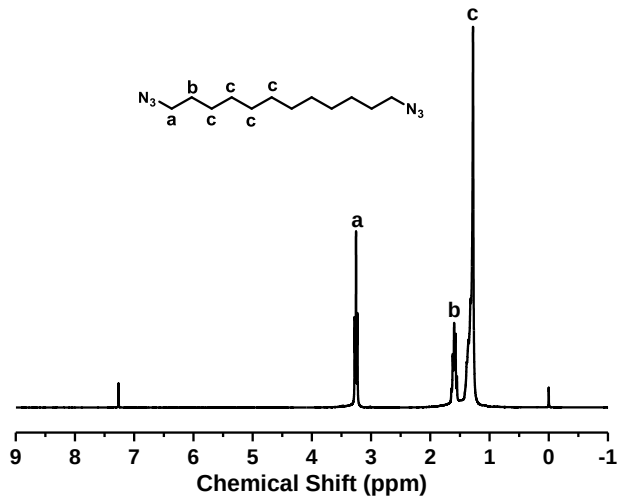

Fig. S4 ^{1}H NMR spectrum of 1,12-diazidododecane at 25 °C in $CDCl_3$.

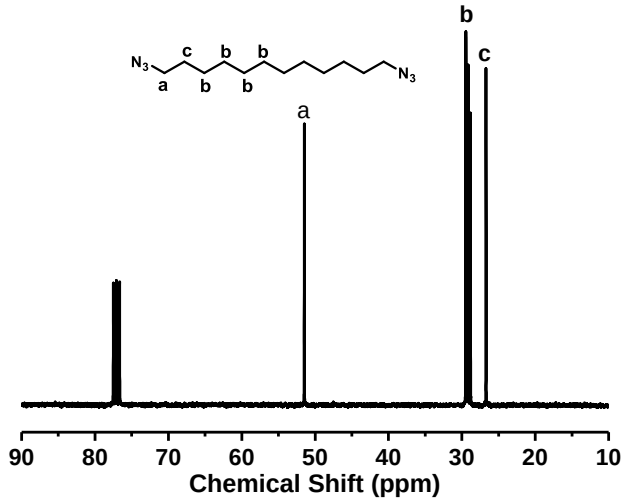

Fig. S5 ^{13}C NMR spectrum of 1,12-diazidododecane at 25 °C in $CDCl_3$.

Synthesis of 1,4-bis(azidomethyl)benzene[2]

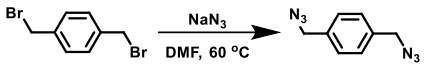

Scheme S3 Synthetic route of 1,4-bis(azidomethyl)benzene.

The synthesis and postpurification procedures for 1,4-bis(azidomethyl)benzene were similar to those of 1,12-diazidododecane, except that 1,4-bis(bromomethyl)benzene (3.001 g, 11.37 mmol) was used to react with NaN_3 (1.773 g, 27.28 mmol). The yield of 1,4-bis(azidomethyl)benzene was 2.03 g (95%), and its structure was verified by ^{1}H NMR and ^{13}C NMR spectroscopy.

^{1}H NMR (300 MHz, $CDCl_3$), δ (TMS, ppm): δ 7.34 (s, 4H), 4.35 (s, 4H). ^{13}C NMR (75 MHz, $CDCl_3$) δ ppm: 135.68, 128.78, 54.53.

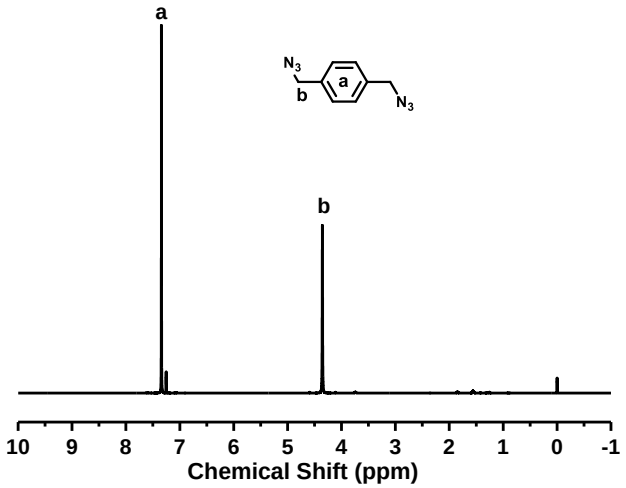

Fig. S6 ^{1}H NMR spectrum of 1,4-bis(azidomethyl)benzene at 25 °C in $CDCl_3$.

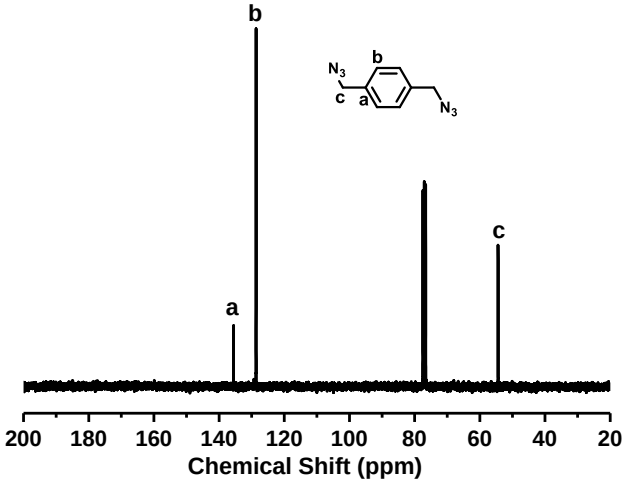

Fig. S7 ^{13}C NMR spectrum of 1,4-bis(azidomethyl)benzene at 25 °C in $CDCl_3$.

Synthesis of 2,7-diazido-9,9-dioctyl-9H-fluorene[3]

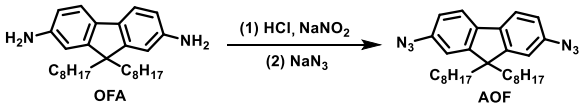

Scheme S4 Synthetic route of 2,7-diazido-9,9-dioctyl-9*H*-fluorene.

9,9-dioctyl-9*H*-fluorene-2,7-diamine was dissolved in a mixture of water (90 mL) and hydrochloric acid (36 mL) at 0 °C. The solution of $NaNO_2$ (4.002 g, 58.0 mmol) in water was added dropwise to the above mixture at 0-5 ºC with stirring. After the mixture was kept below 5 °C with a magnetic stirring for 1 h, a solution of NaN_3 (0.5981 g, 9.2 mmol) in water was added dropwise while the temperature was kept below 5 °C. Then the mixture was stirred at 0 °C for 4 h. And the mixture was extracted with DCM (6 × 30 mL). After the organic layer was washed with water and brine, it was dried over anhydrous Na_2SO_4 and filtered. The filtrate was concentrated by rotary evaporation. The concentrate was purified by silica gel column chromatography using n-hexane as the eluent. The product was abstained as yellow liquid (1.63 g, yield: 86%).

^{1}H NMR (300 MHz, $CDCl_3$), δ (TMS, ppm): δ 7.60 (d, 2H), 7.03-6.97 (dd, 2H), 6.96-6.93 (d, 2H), 1.97-1.87 (m, 4H), 1.34-0.99 (m, 20H), 0.86-0.79 (t, 6H), 0.58 (dd, 4H). ^{13}C NMR (75 MHz, $CDCl_3$) δ ppm: 152.58, 138.74, 137.61, 120.54, 117.88, 113.59, 55.46, 40.38, 31.77, 29.89, 29.19, 23.65, 22.59, 14.06.

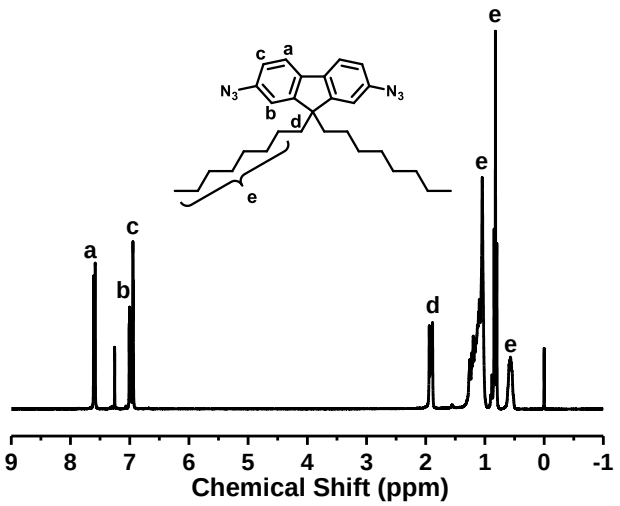

Fig. S8 ^{1}H NMR spectrum of 2,7-diazido-9,9-dioctyl-9*H*-fluorene at 25 °C in $CDCl_3$.

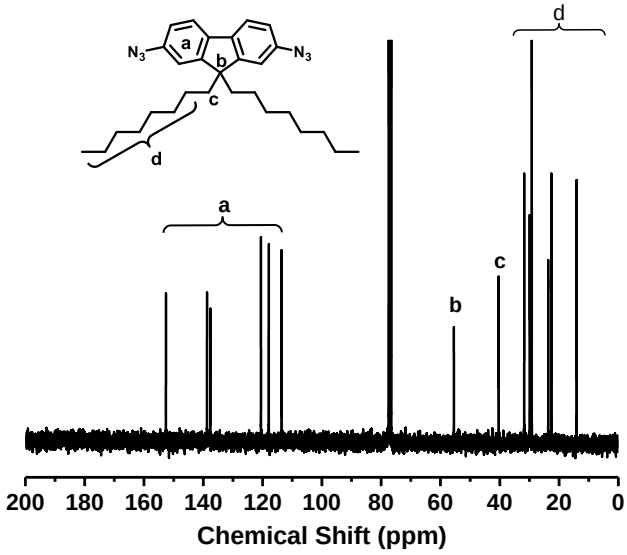

Fig. S9 ^{13}C NMR spectrum of 2,7-diazido-9,9-dioctyl-9*H*-fluorene at 25 °C in $CDCl_3$.

Synthesis of 11-azidoundecanoic acid[4]

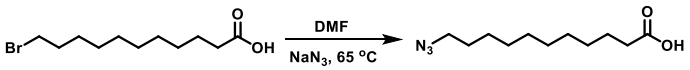

Scheme S5 Synthetic route of 11-azidoundecanoic acid.

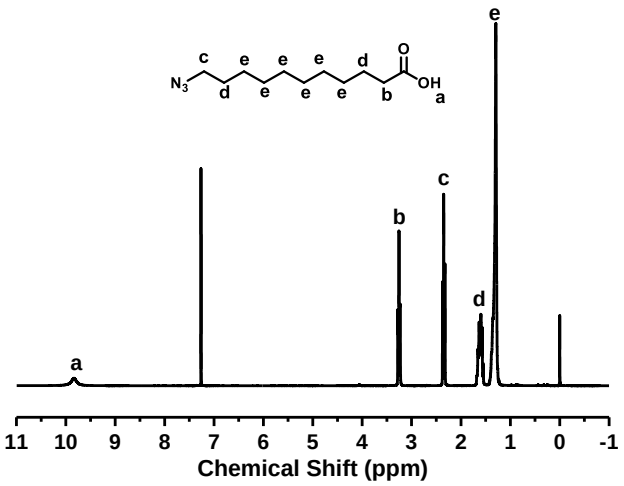

Fig. S10 ^{1}H NMR spectrum of 11-azidoundecanoic acid at 25 °C in $CDCl_3$

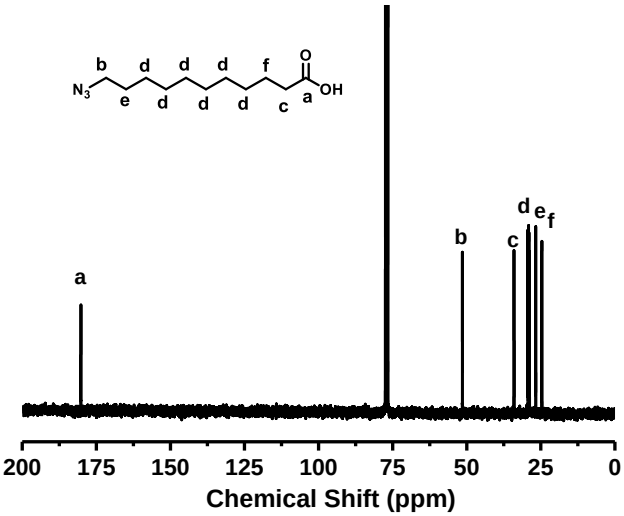

Fig. S11 ^{13}C NMR spectrum of 11-azidoundecanoic acid at 25 °C in $CDCl_3$.

2. Polyamidation of Diacids and Diazides via the Catalytic Staudinger-Vilarrasa Reaction

1) Solvent Screening of Polyamidation

Table S1 Solvent Screening for Polyamidation of Diacids and Diazides via the Catalytic S-V Reaction.[a]

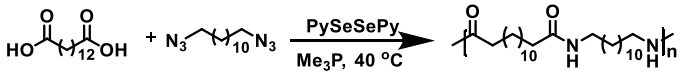

entry	solvent	$M_{n,NMR}$ (Da)[b]	yield (%)[c]
1	toluene/DMF (v/v = 1/1)	28400	89
2	toluene/DMF(LiBr) (v/v = 1/1)	8200	71
3	toluene/NMP (v/v = 1/1)	31800	73
4	toluene/HMPA (v/v = 1/1)	17500	77
5	toluene/anisole (v/v = 1/1)	29300	87
6	toluene/1,4-dioxane (v/v = 1/1)	31800	83
7	toluene	32700	94

[a] Reaction conditions: 0.5 mmol tetradecanedioic acid, 0.5 mmol 1,12-diazidododecane, 0.2 mmol PySeSePy and 1.2 mL cosolvent are added into reaction tube and then added 1.2 mL of 1.0 M toluene solution of Me_3P at 0 °C in a glovebox, then heated to 40 °C when gas bubbles were no longer observed. [b] Determined by ^{1}H NMR of the polyamides. [c] Determined by gravimetric analysis after the crude products are dissolved using HFIP and then precipitated in methanol.

2) Results and Discussion

Table S2 Synthesis of Polyamides via the Catalytic S-V Reaction.

entry	polymer	diacids	diazides	yield (%)[a]	M_n (Da)[b]	$Đ$[b]
1	PA-1220		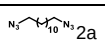 2a	82	28000	2.16
2	PA-1214	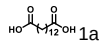 1a	2a	94	27800	1.67
3	PA-1212		2a	92	6000	2.69
4	PA-1210		2a	92	6000	2.16
5	PA-128		2a	82	3500	1.13
6	PA-127		2a	81	3800	1.16
7	PA-125		2a	58	4500	1.17
8	PA-124		2a	72	3400	1.15
9	PA-123		2a	49	4600	2.81
10	PA-11			82	3100	1.13
11	PA-AM14	1a	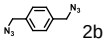 2b	42	2100	1.13
12	PA-AMPPBA	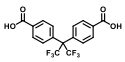	2b	89	1600	1.10
13	PA-AMT	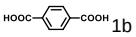 1b	2b	55	2800	1.18
14	PA-AOFT	1b	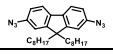	85	3700	2.28

[a] Determined by gravimetric analysis after the crude products were dissolved in HFIP and then precipitated in methanol. [b] The number average molecular weight and polydispersity index determined by SEC with HFIP as the eluent and PMMA as the calibration standard.

The structure of PA1220 was characterized by ^{1}H NMR (Fig. S12). As presented in Fig. S12, the resonance signal at 5.90 ppm in the ^{1}H NMR spectrum is attributed to the amide proton, indicating the successful formation of the amide bond. In addition, the area integral of each peak in the ^{1}H NMR spectrum matches well with the number of magnetically different protons corresponding to the repeating unit structure of the obtained polymer. Therefore, the ^{1}H NMR analysis indicated the occurrence of the azide-acid click polymerization.

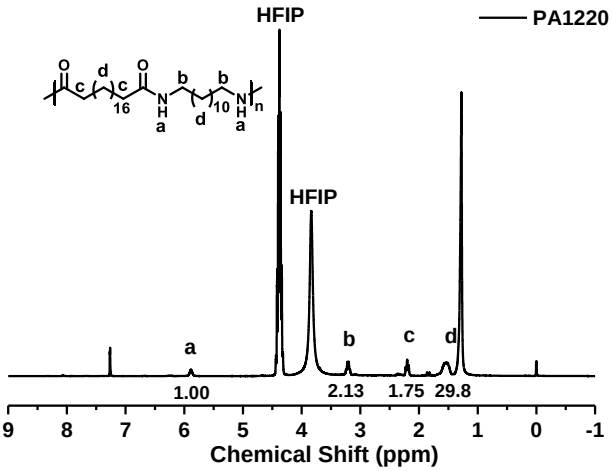

Fig. S12 ^{1}H NMR spectrum of the PA1220 in HFIP and $CDCl_3$ (V/V = 1/3) (Table S2, entry 1).[5]

The structure of PA1212 was characterized by ^{1}H NMR (Fig. S13). As presented in Fig. S13, the resonance signal at 5.88 ppm in the ^{1}H NMR spectrum is attributed to the amide proton, indicating the successful formation of the amide bond. In addition, the area integral of each peak in the ^{1}H NMR spectrum matches well with the number of magnetically different protons corresponding to the repeating unit structure of the obtained polymer. Therefore, the ^{1}H NMR analysis indicated the occurrence of the azide-acid click polymerization.

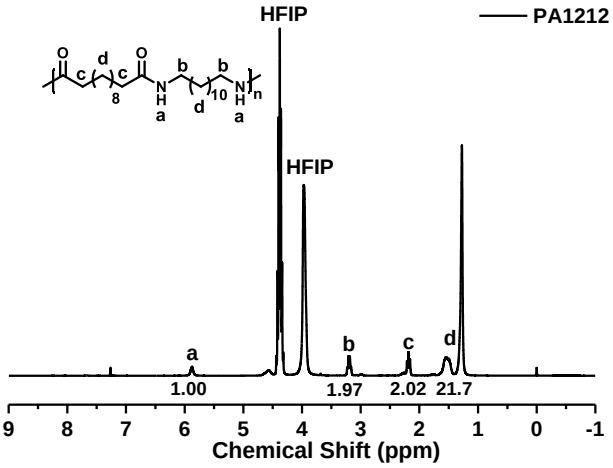

Fig. S13 ^{1}H NMR spectrum of the PA1212 in HFIP and $CDCl_3$ (V/V = 1/3) (Table S2, entry 3).

The structure of PA1210 was characterized by ^{1}H NMR (Fig. S14). As presented in Fig. S14, the resonance signal at 5.87 ppm in the ^{1}H NMR spectrum is attributed to the amide proton, indicating the successful formation of the amide bond. In addition, the area integral of each peak in the ^{1}H NMR spectrum matches well with the number of magnetically different protons corresponding to the repeating unit structure of the obtained polymer. Therefore, the ^{1}H NMR analysis indicated the occurrence of the azide-acid click polymerization.

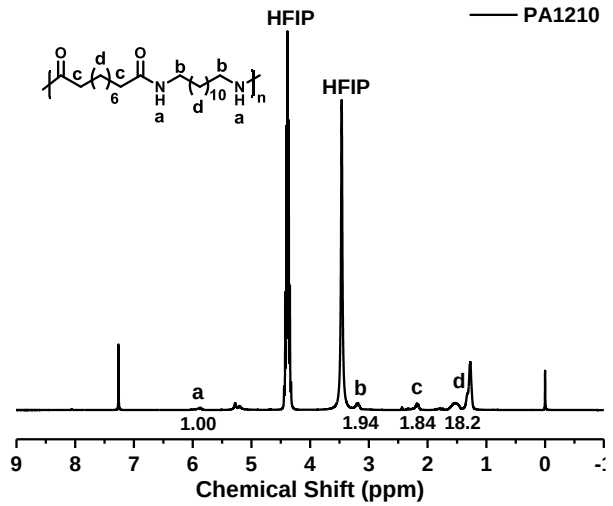

Fig. S14 ^{1}H NMR spectrum of the PA1210 in HFIP and $CDCl_3$ (V/V = 1/3) (Table S2, entry 4).

The structure of PA128 was characterized by ^{1}H NMR (Fig. S15). As presented in Fig. S15, the resonance signal at 5.92 ppm in the ^{1}H NMR spectrum is attributed to the amide proton, indicating the successful formation of the amide bond. In addition, the area integral of each peak in the ^{1}H NMR spectrum matches well with the number of magnetically different protons corresponding to the repeating unit structure of the obtained polymer. Therefore, the ^{1}H NMR analysis indicated the occurrence of the azide-acid click polymerization.

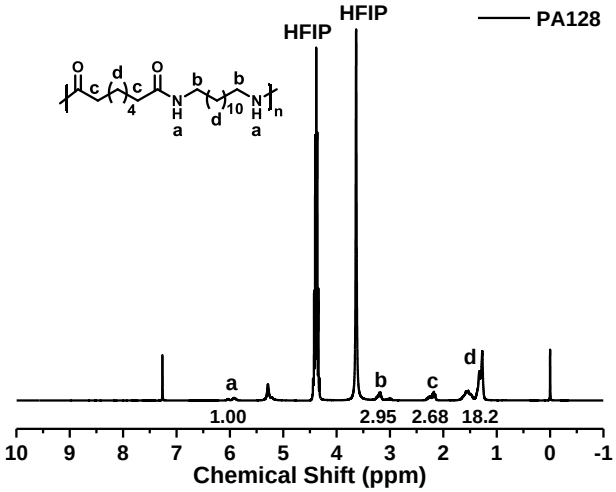

Fig. S15 ^{1}H NMR spectrum of the PA128 in HFIP and $CDCl_3$ (V/V = 1/3) (Table S2, entry 5).

The structure of PA127 was characterized by ^{1}H NMR (Fig. S16). As presented in Fig. S16, the resonance signal at 5.94 ppm in the ^{1}H NMR spectrum is attributed to the amide proton, indicating the successful formation of the amide bond. In addition, the area integral of each peak in the ^{1}H NMR spectrum matches well with the number of magnetically different protons corresponding to the repeating unit structure of the obtained polymer. Therefore, the ^{1}H NMR analysis indicated the occurrence of the azide-acid click polymerization.

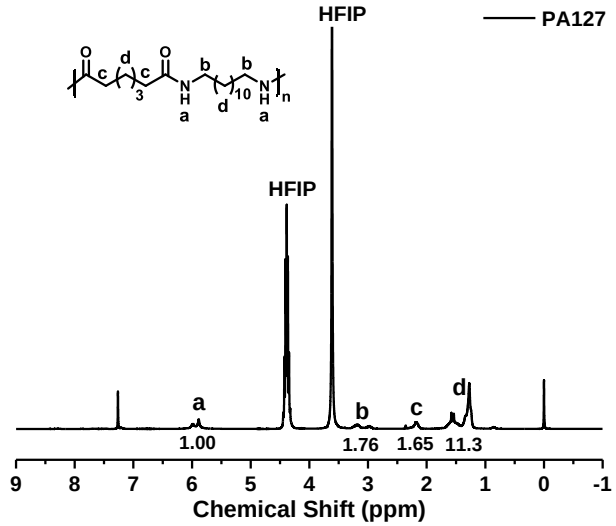

Fig. S16 ^{1}H NMR spectrum of the PA127 in HFIP and $CDCl_3$ (V/V = 1/3) (Table S2, entry 6).

The structure of PA125 was characterized by ^{1}H NMR (Fig. S17). As presented in Fig. S17, the resonance signal at 6.10 ppm in the ^{1}H NMR spectrum is attributed to the amide proton, indicating the successful formation of the amide bond. In addition, the area integral of each peak in the ^{1}H NMR spectrum matches well with the number of magnetically different protons corresponding to the repeating unit structure of the obtained polymer. Therefore, the ^{1}H NMR analysis indicated the occurrence of the azide-acid click polymerization.

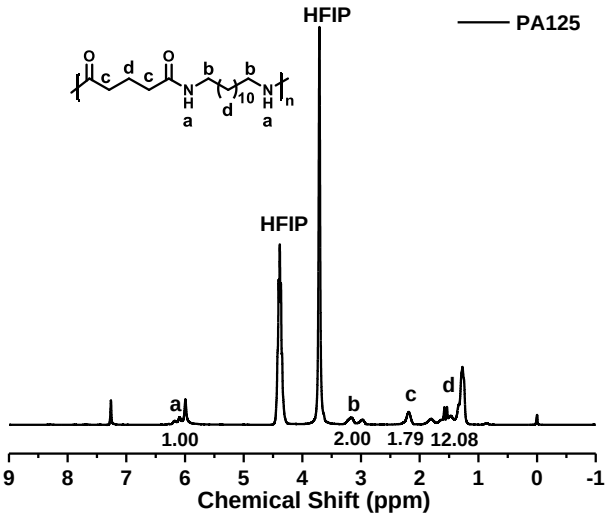

Fig. S17 ^{1}H NMR spectrum of the PA125 in HFIP and $CDCl_3$ (V/V = 1/3) (Table S2, entry 7).

The structure of PA124 was characterized by ^{1}H NMR (Fig. S18). As presented in Fig. S18, the resonance signal at 6.08 ppm in the ^{1}H NMR spectrum is attributed to the amide proton, indicating the successful formation of the amide bond. In addition, the area integral of each peak in the ^{1}H NMR spectrum matches well with the number of magnetically different protons corresponding to the repeating unit structure of the obtained polymer. Therefore, the ^{1}H NMR analysis indicated the occurrence of the azide-acid click polymerization.

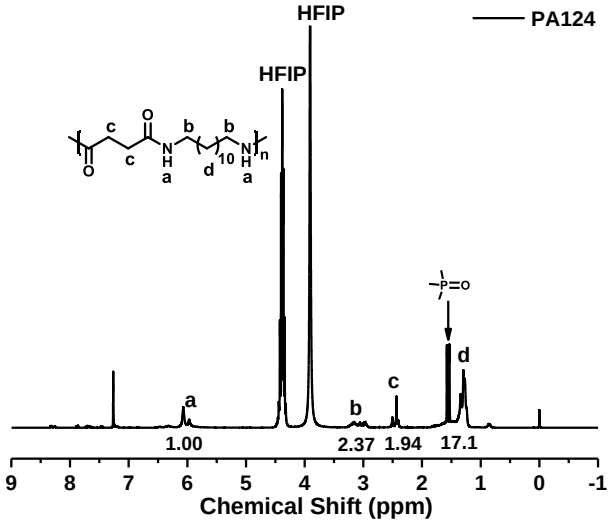

Fig. S18 ^{1}H NMR spectrum of the PA124 in HFIP and $CDCl_3$ (V/V = 1/3) (Table S2, entry 8).

The structure of PA123 was characterized by ^{1}H NMR (Fig. S19). As presented in Fig. S19, the resonance signal at 5.95 ppm in the ^{1}H NMR spectrum was is attributed to the amide proton, indicating the successful formation of the amide bond. In addition, the area integral of each peak in the ^{1}H NMR spectrum matches well with the number of magnetically different protons corresponding to the repeating unit structure of the obtained polymer. Therefore, the ^{1}H NMR analysis indicated the occurrence of the azide-acid click polymerization.

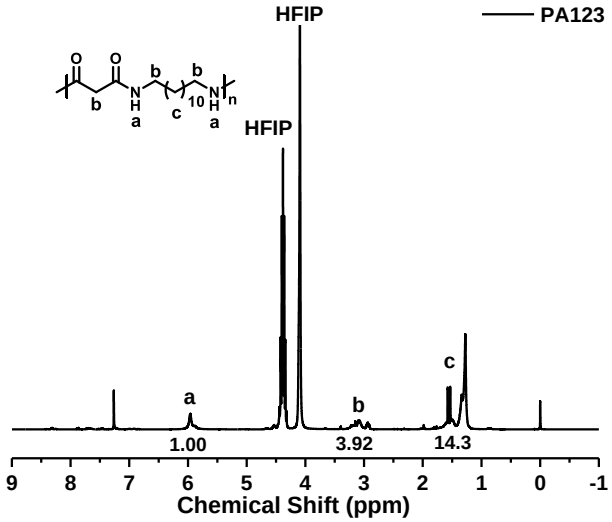

Fig. S19 ^{1}H NMR spectrum of the PA123 in HFIP and $CDCl_3$ (V/V = 1/3) (Table S2, entry 9).

The structure of PA11 was characterized by ^{1}H NMR (Fig. S20). As presented in Fig. S20, the resonance signal at 6.04 ppm in the ^{1}H NMR spectrum is attributed to the amide proton, indicating the successful formation of the amide bond. In addition, the area integral of each peak in the ^{1}H NMR spectrum matches well with the number of magnetically different protons corresponding to the repeating unit structure of the obtained polymer. Therefore, the ^{1}H NMR analysis indicated the occurrence of the azide-acid click polymerization.

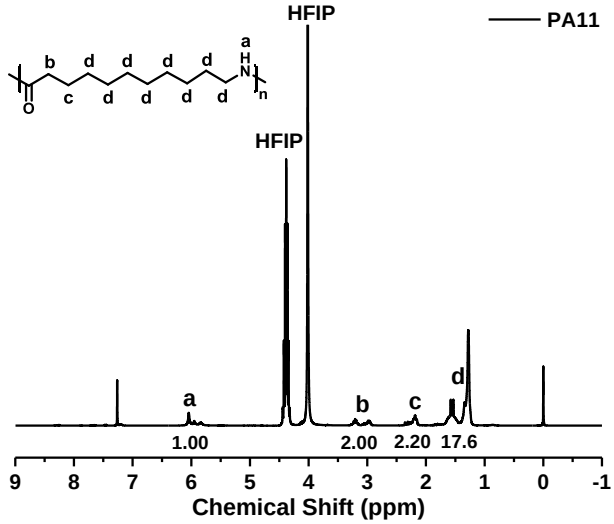

Fig. S20 ^{1}H NMR spectrum of the PA11 in HFIP and $CDCl_3$ (V/V = 1/3) (Table S2, entry 10).

The structure of PA-AM14 was characterized by ^{1}H NMR (Fig. S21). As presented in Fig. S21, the resonance signal at 6.17 ppm in the ^{1}H NMR spectrum is attributed to the amide proton, indicating the successful formation of the amide bond. In addition, the area integral of each peak in the ^{1}H NMR spectrum matches well with the number of magnetically different protons corresponding to the repeating unit structure of the obtained polymer. Therefore, the ^{1}H NMR analysis indicated the occurrence of the azide-acid click polymerization.

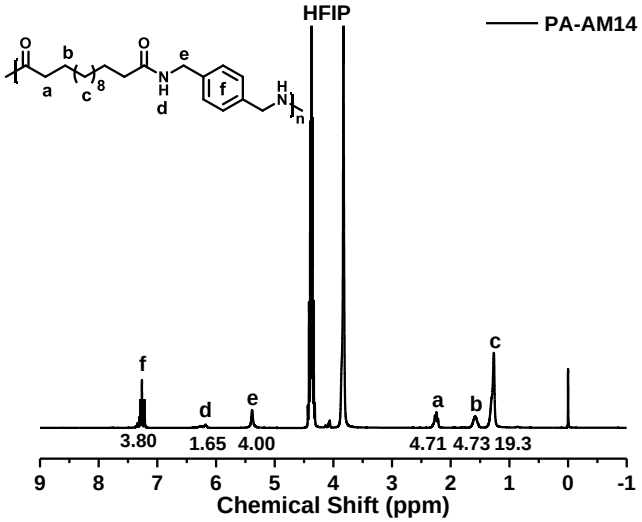

Fig. S21 ^{1}H NMR spectrum of the PA-AM14 in HFIP and $CDCl_3$ (V/V = 1/3) (Table S2, entry 11).

The structure of PA-AOFT was characterized by ^{1}H NMR (Fig. S22). As presented in Fig. S22, the resonance signal at 6.86 ppm in the ^{1}H NMR spectrum is attributed to the amide proton, indicating the successful formation of the amide bond. In addition, the area integral of each peak in the ^{1}H NMR spectrum matches well with the number of magnetically different protons corresponding to the repeating unit structure of the obtained polymer. Therefore, the ^{1}H NMR analysis indicated the occurrence of the azide-acid click polymerization.

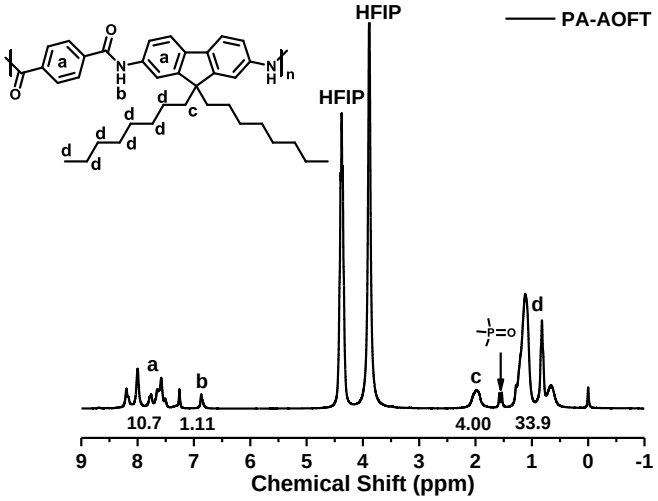

Fig. S22 ^{1}H NMR spectrum of the PA-AOFT in HFIP and $CDCl_3$ (V/V = 1/3) (Table S2, entry 14).

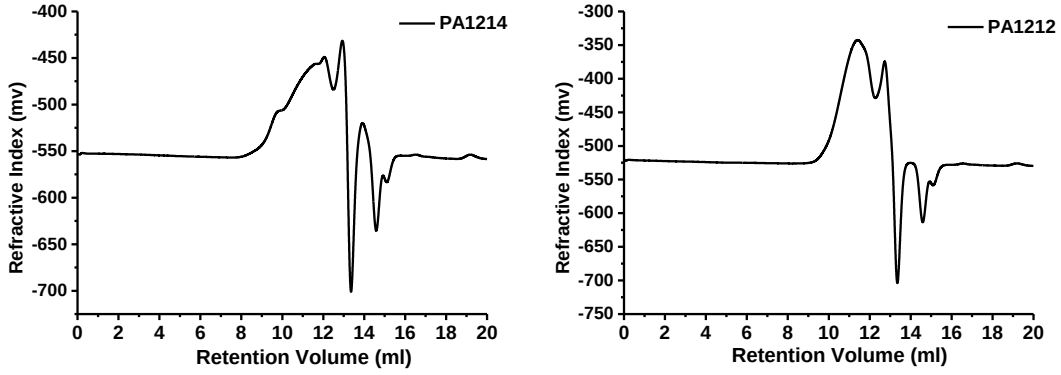

Fig. S23 SEC curves of PA1214 and PA1212. HFIP was used as the eluent and PMMA standards as the calibration.[5,6]

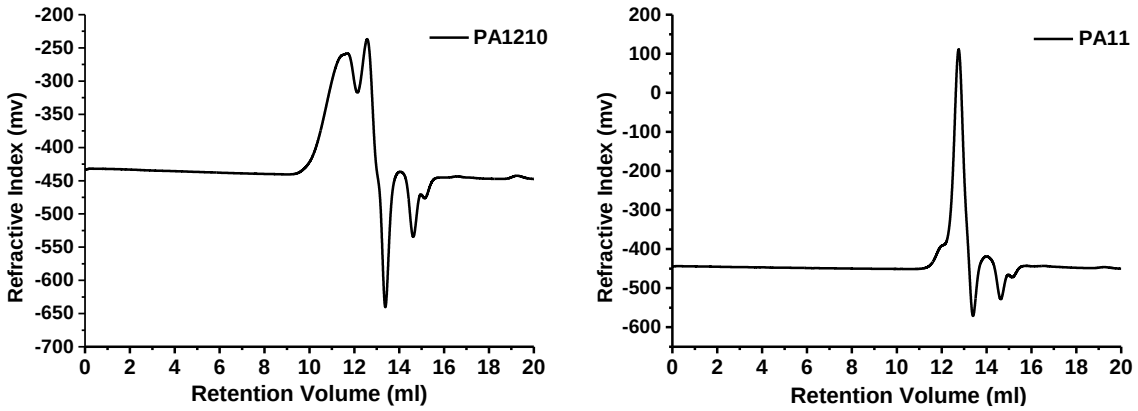

Fig. S24 SEC curves of PA1210 and PA11. HFIP was used as the eluent and PMMA standards as the calibration.

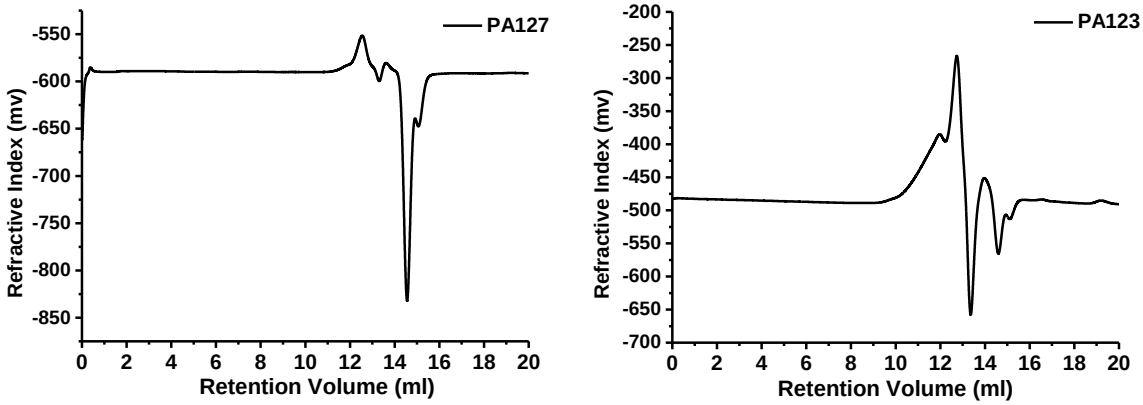

Fig. S25 SEC curves of PA127 and PA123. HFIP was used as the eluent and PMMA standards as the calibration.

Section B. Acylation Reaction of the End Group of Polymers.

1. The Acylation Reaction of End Group of Polymer-N_3 and N_3-Polymer-N_3

1) Synthesis and Characterization of Polymer-N_3 and N_3-Polymer-N_3[7]

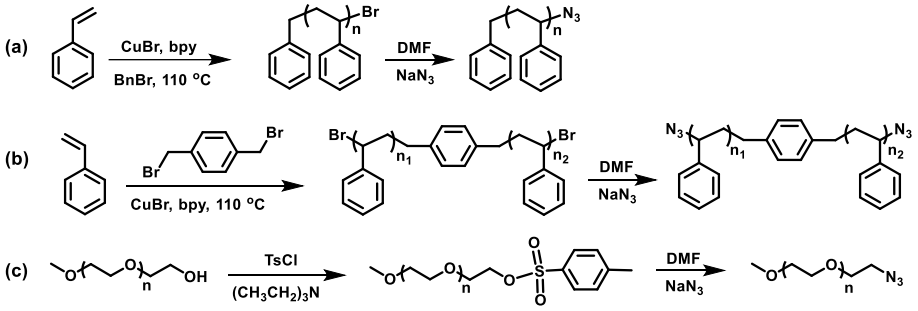

Scheme S6. Schematic illustration of synthesis of (a) PS-N_3, (b) N_3-PS-N_3 and (c) PEG-N_3

Synthesis of PS-N_3. In a dry 50 mL Schlenk flask CuBr (0.2505 g, 1.746 mmol) and bipyridene (0.8181 g, 5.238 mmol), benzyl bromide (0.4479 g, 2.619mmol) was mixed together. Then styrene (18.18 g, 174.6 mmol) was injected into the mixture, followed sealing with a rubber bung. The mixture was degassed by three consecutive freeze-pump-haw cycles and was placed into an oil bath at 110 °C with stirring. After 75 minutes, the reaction was stopped and the flask was allowed to cool to room temperature. Then the mixture was dissolved in THF and the solution was filtered through a neutral alumina column to remove the catalyst. The filtrate was precipitated in excess of cold methanol. The polymer was obtained by filtration and dried in a vacuum oven overnight to afford white solid. (PS-Br, 5.1 g, yield: 27%, M_n = 3200 Da, $Đ$ = 1.22).

PS-Br (4.0 g, 1.25 mmol), NaN_3 (0.8126 g, 12.5 mmol) and DMF (35 mL) were added into a 100 mL round-bottom flask. Then the mixture was placed in an oil bath at 60 °C with a magnetic stirring for 24 h. After cooling to room temperature, the mixture was passed through a neutral alumina column to remove residual sodium salts. Then the solution was precipitated into an excess of cold methanol. The obtained product was dried overnight in a vacuum oven for 24 h (PS-N_3, 3.4 g, yield: 85%, M_n = 3400 Da, $Đ$ = 1.20).

Synthesis of N_3-PS-N_3. The polymerization was conducted in a dry Schlenk tube under argon atmosphere. Styrene (5.454 g, 0.0524 mol) was injected into the dry Schlenk tube with CuBr (0.2146 g, 1.496 mmol), bipyridene (0.4673 g, 2.992 mmol) and 1,4-bis(bromomethyl)benzene (0.3949 g, 1.496 mmol). The tube was degassed by three consecutive freeze-pump-thaw cycles and was placed into an oil bath at 110 °C with stirring for 60 min. Then the mixture was cooled to room temperature and discovered in THF. After passing through a neutral alumina column to remove the catalyst, the solution was precipitated in excess of cold methanol. The resultant polymer was collected by filtration and dried in a vacuum oven overnight to afford white power, which was then submitted for SEC and ^{1}HNMR tests (Br-PS-Br, 4.1 g, yield: 70%, M_n = 3800 Da, $Đ$ = 1.24).

Br-PS-Br (4.0 g, 1.053 mmol) and NaN_3 (1.368 g, 21.06 mmol) were added to a 100 mL round-bottom flask with a magnetic stirrer and discovered in 40 mL DMF. Then the mixture was placed in an oil bath at 60 °C with a magnetic stirring for 48 h. After cooling to room temperature, the mixture was discovered in THF and then passed through a neutral alumina column to remove residual sodium salts. Then the solution was precipitated into an excess of cold methanol. The white product was obtained by filtering and dried overnight in a vacuum oven (N_3-PS-N_3, 4.1 g, yield: 80%, M_n = 3900 Da, $Đ$ = 1.19).

Synthesis of poly(ethyleneglycol) methylether azide (PEG-N_3). Poly(ethylene glycol) methyl ether (15.00 g, 7.895 mmol) was added to a 500 mL round-bottom flask and was dissolved in 200 mL DCM. After triethylamine (7.989 g, 78.95 mmol) were added, the flask was placed into in an ice salt bath with a magnetic stirrer which must keep approximately 0 °C. The solution of 4-methylbenzenesulfonyl chloride (TsCl) (15.05 g, 78.95 mmol) in 100 mL DCM was added dropwise to the above mixture through the addition funnel. Then the reaction mixture was warmed gradually to room temperature and was stirred for 24 h. Afterwards, the reaction mixture was filtered, concentrated to remove most the solvent and precipitated into an excess of cold diethyl ether. The polymer was obtained by filtration and dried in a vacuum oven overnight to afford white solid (PEG-OTs, 14.0 g, yield: 86%).

PEG-OTs (14.00 g, 7.000 mmol), NaN_3 (4.551 g, 70.00 mmol) and DMF (60 mL) were added into a 100 mL round-bottom flask with a magnetic stirrer. The flask was placed in an oil bath at 80 °C for 24 h. After cooling to room temperature, the mixture was passed through a neutral alumina column to remove residual sodium salts. Then 400 mL chloromethane was added to the above filtrate. The mixture was washed with saturated NH_4Cl solution, water and brine. The organic layer was dried with anhydrous sodium sulfate, concentrated to remove most the solvent and precipitated into an excess of cold diethyl ether. The polymer was obtained by filtration and dried in a vacuum oven overnight to afford white solid (PEG-N_3, 11.3 g, yield: 86%, M_n = 2600 Da, $Đ$ = 1.04).

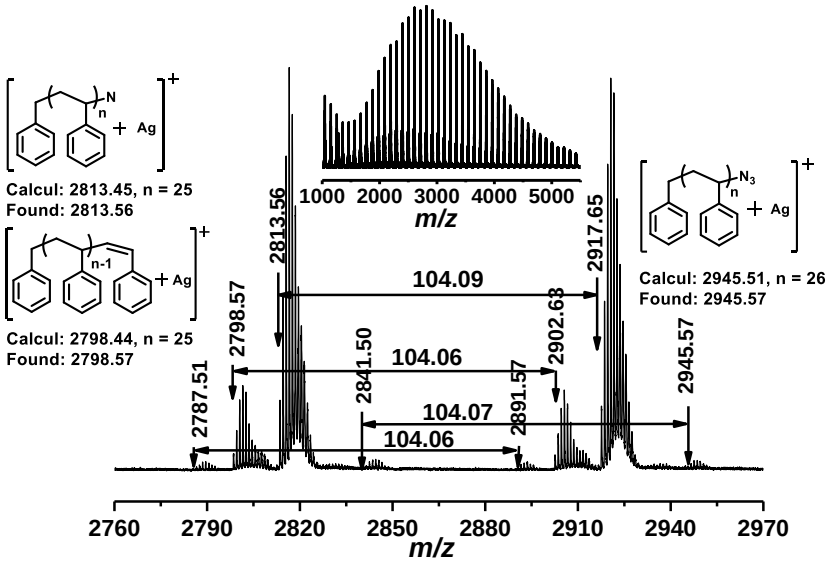

Fig. S26 MALDI-TOF-MS spectrum of PS-N_3 obtained through the reaction of PS-Br with NaN_3.

As shown in Fig. S26, all the experimental mass match well with the theoretical value, except the weakest peak at 2787.51 Da. The experimental mass (2945.57 Da) of PS-N_3 is in accordance with theoretical value (2945.51 Da, n = 26, with Ag^+). Moreover, PS-N_3 exhibits two distinct distributions in the MALDI-TOF-MS spectrum when analyzed using reflector mode detection. One is the fragment ions of ([PS-N+Ag] $^+$) resulting from a loss of N_2 of PS-N_3. The other is the fragment ions of PS-macromonomer (experimental mass = 2798.57 Da and theoretical value = 2798.44 Da, n = 25, with Ag^+) with an unsaturated C=C bond. Because the carbon-bromine bond of PS-Br was so weak that the bond could be cleaved to generate the fragment of PS-macromonomer during the MALDI-TOF-MS analysis.[8] Therefore, it was not rigorous to characterize the PS-N_3 only by MALDI-TOF-MS.

To verify the azide chain-end fidelity, both PS-Br and PS-N_3 were analyzed by ^{1}H NMR (Fig. S27a). As shown in Fig. S27a, the spectrum clearly shows the shift of the resonance for the proton next to the bromine end group from 4.45 ppm (PS-Br) to 3.94 ppm (PS-N_3), which also confirms successful substitution.

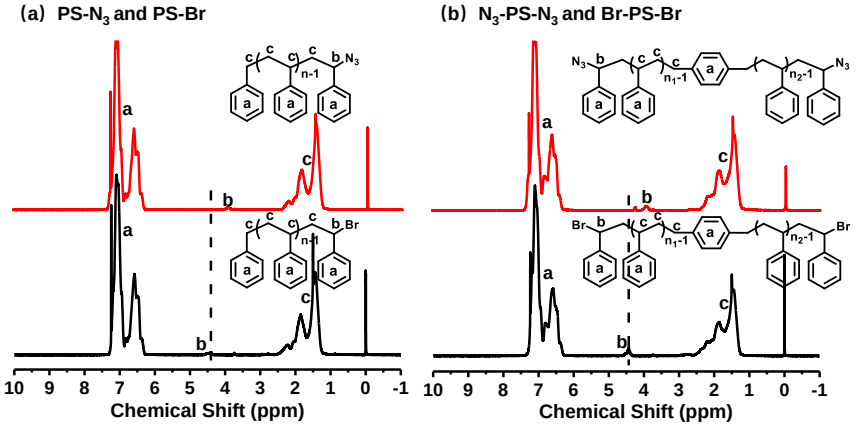

Fig. S27 ^{1}H NMR spectra of (a) PS-N_3 and PS-Br; (b) N_3-PS-N_3 and Br-PS-Br at 25 °C in $CDCl_3$.

As shown in Fig. S27b, the spectrum clearly shows the shift of the resonance for the proton next to the bromine end group from 4.46 ppm (Br-PS-Br) to 3.96 ppm (N_3-PS-N_3), which confirms successful substitution reaction.

Fig. S28 shows the MALDI-TOF-MS spectrum of N_3-PS-N_3. N_3-PS-N_3 exhibits four obvious distributions in the MALDI-TOF-MS spectrum when analyzed using reflector mode detection. The fragment ions of $[N_3\text{-PS-}N_3+Ag]^+$ (experimental mass = 1960.24 Da and theoretical value = 1959.92 Da, $n_1+n_2 = 16$) are observed in the MALDI-TOF-MS spectrum. Three other experimental mass match well with the theoretical value, which are generated during the MALDI-TOF-MS analysis. According to the analysis results by ^{1}H NMR and MALDI-TOF-MS spectra (Fig. S27b and S28), we confirmed that the chain-end functionality of N_3-PS-N_3 was approximately 99%.

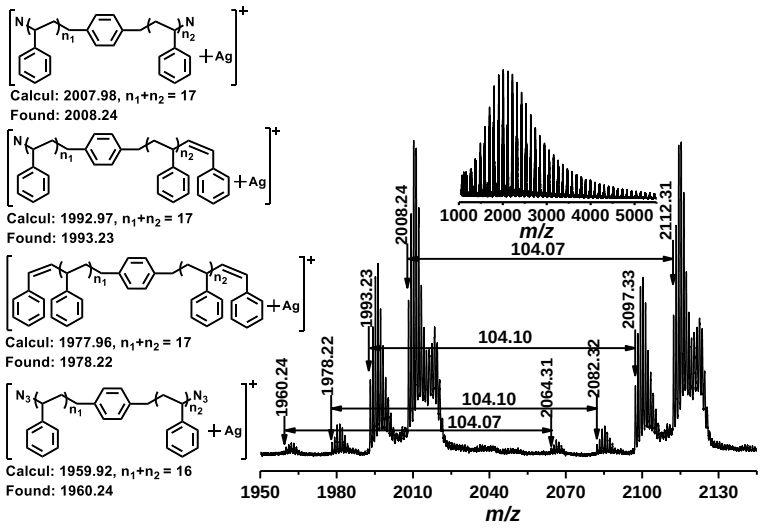

Fig. S28 MALDI-TOF-MS spectrum of N_3-PS-N_3 obtained through the reaction of Br-PS-Br with NaN_3.

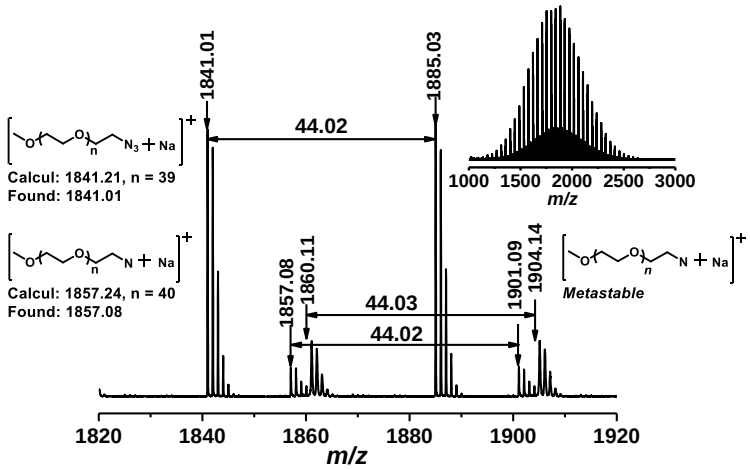

Fig. S29 MALDI-TOF-MS spectrum of PEG-N_3 obtained through the reaction of PEG-OTs with NaN_3.

Fig. S29 shows the MALDI-TOF-MS spectrum of PEG-N_3. PEG-N_3 exhibits three distinct distributions in the MALDI-TOF-MS spectrum when analyzed using reflector mode detection. The fragment ions of $[PEG\text{-}N_3+Na]^+$ (experimental mass = 1841.01 Da and theoretical value = 1841.21 Da, n = 39) are observed in the MALDI-TOF-MS spectrum. The rest of two fragment ions are $[PEG\text{-}N+Na]^+$ (experimental mass = 1857.08 Da and theoretical value = 1857.24 Da, n = 40) and metastable ions (experimental mass = 1904.14 Da) resulting from the expulsion of N_2 by both in-source and the postsource metastable ion formation.[9] The postsource metastable ions are identified by a nonuniform, noninteger mass offset relative to the parent ion ($[PEG\text{-}N_3+Na]^+$), and can be the strongest confirmed by their disappearance in in linear mode detection.[9] In addition, no other indeterminate polymer peak distribution is observed in the MALDI-TOF-MS spectrum, indicating that the PEG-N_3 was the only product.

2) Results and Discussion

Table S3 Time-Dependence of the Amidation Reaction between the End Group of PS-N_3 with Piperonylic Acid.[a]

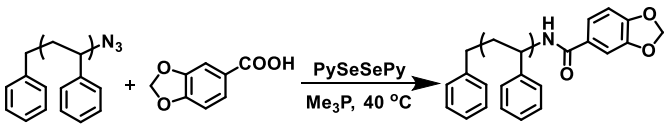

entry	equiv of PS-N_3	equiv of piperonylic acid	equiv of PySeSePy	solvent	time (h)	yield (%)[b]
1	1.0	1.5	0.2	toluene	2	30
2	1.0	1.5	0.2	toluene	6	60
3	1.0	1.5	0.2	toluene	10	86
4	1.0	1.5	0.2	toluene	24	100

[a] PS-N_3 (0.3400 g, 0.1 mmol), piperonylic acid (0.0332 g, 0.2 mmol), and PySeSePy (0.0126 g, 0.04 mmol) were mixed with 1.5 mL of 1.0 M toluene solution of Me_3P at 0 °C in a glovebox. When no gas was observed, the solution was heated to 40 °C and stirred, monitored, and samples were taken and analyzed by MALDI-TOF-MS. [b] The yield was roughly estimated from the MALDI-TOF-MS spectra with a 10% estimated error.[10]

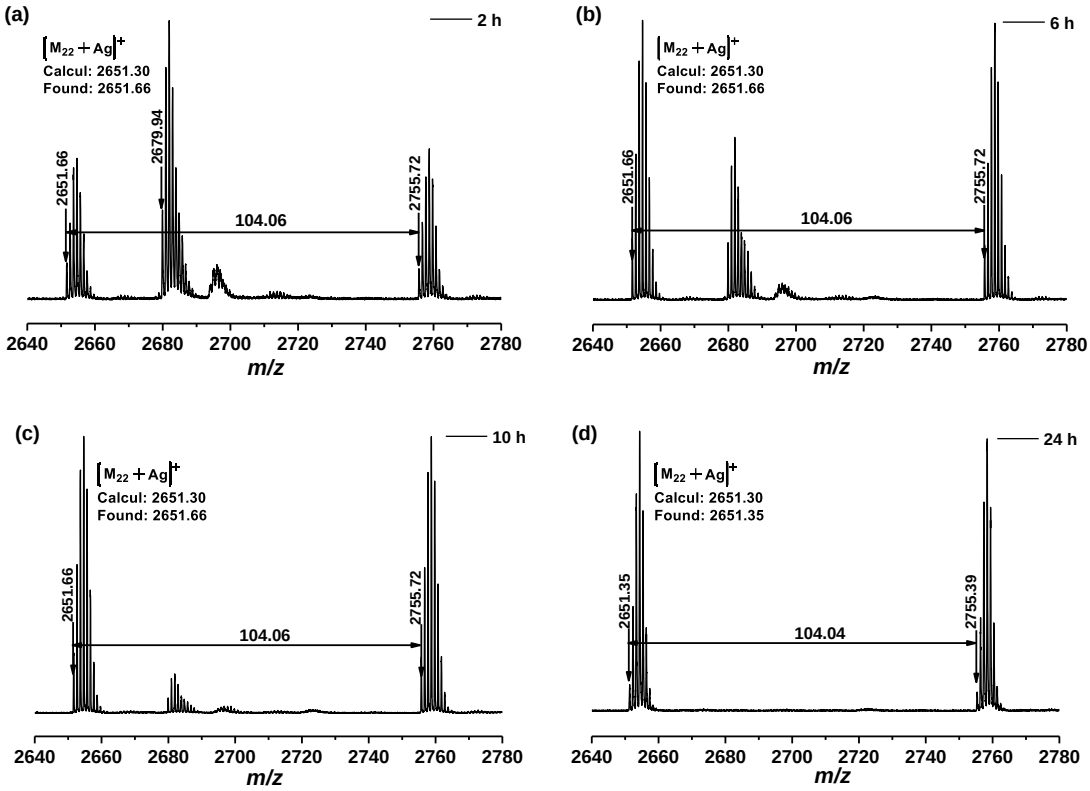

Fig. S30 MALDI-TOF-MS spectra of the polymer obtained during the reaction of PS-N_3 with piperonylic acid at different reaction times.

The acylation reaction of end group of PS-N_3 with anisic acid

The efficiency of amidation reaction was evident in the MALDI-TOF-MS, which shows a single polymer peak distribution corresponding to amide-terminated PS (Fig. S31). Furthermore, the experimental mass (2949.56 Da) matches well with the theoretical value (2949.51 Da, n = 25, with Ag^+). In addition, ^{1}H NMR spectrum of the end amide-functionalized PS further confirmed the high efficiency of the end functionalization (Fig. S32). As shown in Fig. S32, the signal corresponding to the OCH_3 moiety is clearly observed (e, in Fig. S32), which indicates the introduction of the COR moiety on the chain-end of the polystyrene. The chain-end functionality of the product is estimated to be approximately 100% (with ±5% experimental error) from the relative peak areas of the two characteristic peaks (b and e in Fig. S32).

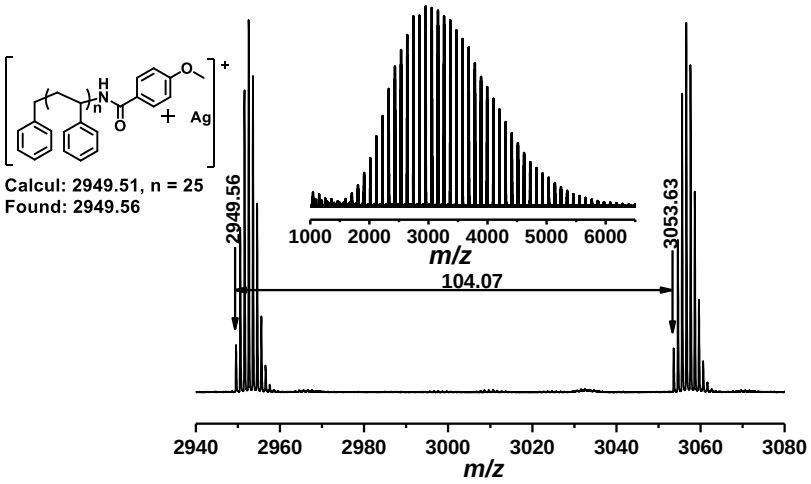

Fig. S31 MALDI-TOF-MS spectrum of the amide-functionalized PS via the catalytic S-V reaction of with anisic acid (Table 2, entry 2).

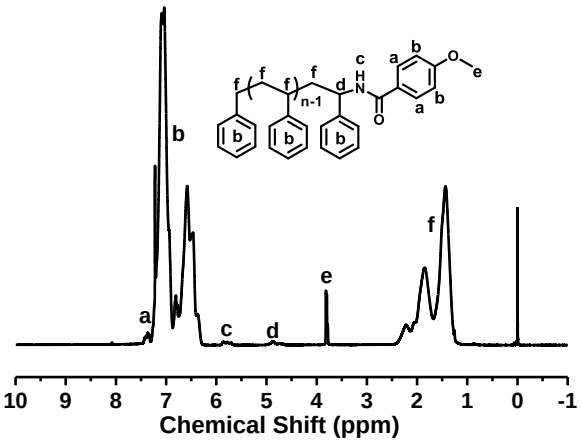

Fig. S32 ^{1}H NMR spectrum of the amide-functionalized PS via the catalytic S-V reaction of PS-N_3 with anisic acid (Table 2, entry 2) at 25 °C in $CDCl_3$.

The acylation reaction of end group of PS-N_3 with 1-(4-methoxy-phenyl)-cyclopropanecarboxylic acid

The efficiency of amidation reaction was evident in the MALDI-TOF-MS, which shows a single polymer peak distribution corresponding to amide-terminated PS (Fig. S33). Furthermore, the experimental mass (3405.35 Da) matches well with the theoretical value (3405.78 Da, n = 29, with Ag^+). In addition, ^{1}H NMR spectrum of the end amide-functionalized PS further confirmed the high efficiency of the end functionalization (Fig. S34). As shown in Fig. S34, the signal corresponding to the OCH_3 moiety is clearly observed (d, in Fig. S34), which indicates the introduction of the COR moiety on the chain-end of the polystyrene. The chain-end functionality of the product is estimated to be approximately 98% (with ±5% experimental error) from the relative peak areas of the two characteristic peaks (d and e in Fig. S34).

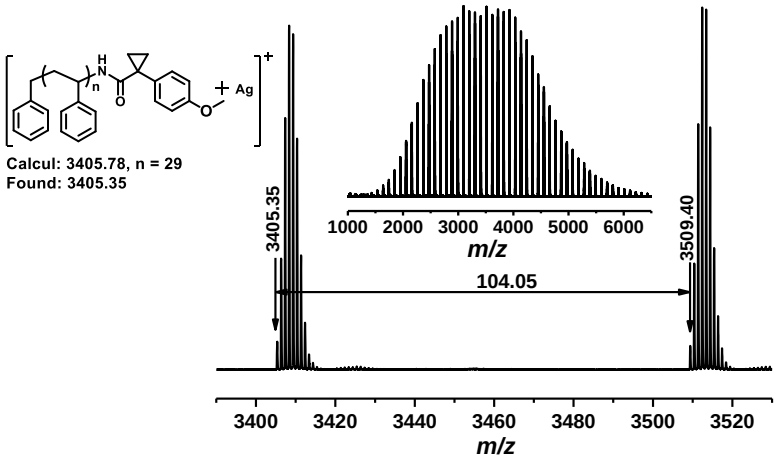

Fig. S33 MALDI-TOF-MS spectrum of the amide-functionalized PS via the catalytic S-V reaction of PS-N_3 with 1-(4-methoxy-phenyl)-cyclopropanecarboxylic acid (Table 2, entry 3).

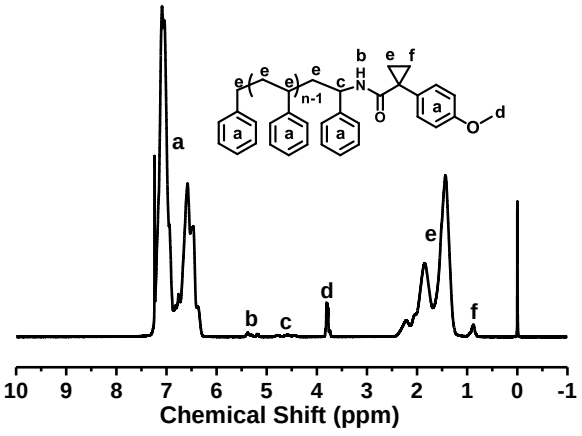

Fig. S34 ^{1}H NMR spectrum of the amide-functionalized PS via the catalytic S-V reaction of PS-N_3 with 1-(4-methoxy-phenyl)-cyclopropanecarboxylic acid (Table 2, entry 3) at 25 °C in $CDCl_3$.

The acylation reaction of end group of PS-N_3 with benzoic acid

Fig. S35 shows the MALDI-TOF-MS spectrum of the end-functionalized PS via the catalytic S-V reaction of PS-N_3 with benzoic acid. Only a single polymer peak distribution is observed, and the experimental mass (2815.89 Da) matches well with the theoretical value (2815.51 Da, n = 24, with Ag^+), demonstrating the high efficient transformation of PS-N_3 into the PS-NH-COR in quantitative.

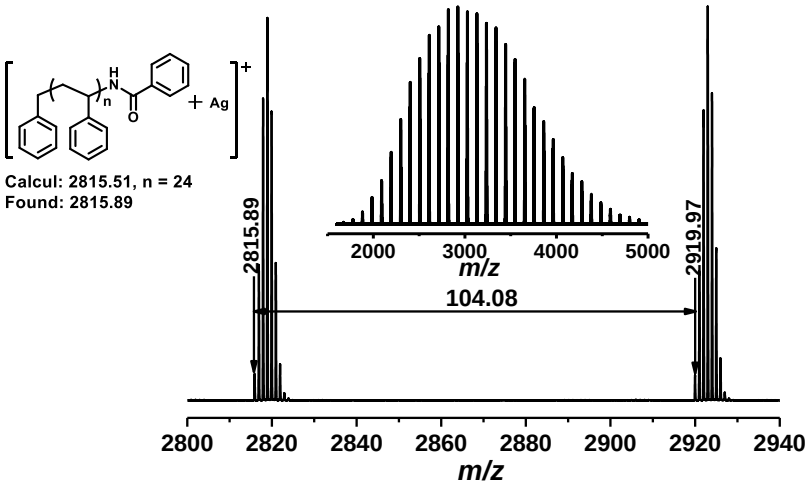

Fig. S35 MALDI-TOF-MS spectrum of the amide-functionalized PS via the catalytic S-V reaction of PS-N_3 with benzoic acid (Table 2, entry 4).

The acylation reaction of end group of PS-N_3 with stearic acid

Fig. S36 shows the MALDI-TOF-MS spectrum of the end-functionalized PS via the catalytic S-V reaction of PS-N_3 with stearic acid. Only a single polymer peak distribution is observed, and the experimental mass (2874.03 Da) matches well with the theoretical value (2873.68 Da, n = 23, with Ag^+), demonstrating the high efficient transformation of PS-N_3 into the PS-NH-COR in quantitative.

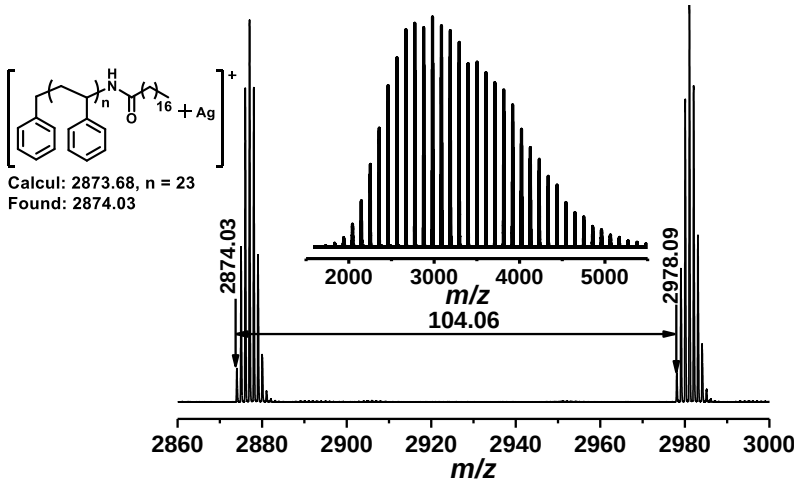

Fig. S36 MALDI-TOF-MS spectrum of the amide-functionalized PS via the catalytic S-V reaction of PS-N_3 with stearic acid (Table 2, entry 5).

The acylation reaction of end group of PS-N_3 with 2-methylhexanoic acid

Fig. S37 shows the MALDI-TOF-MS spectrum of the end-functionalized PS via the catalytic S-V reaction of PS-N_3 with 2-methylhexanoic acid. Only a single polymer peak distribution is observed, and the experimental mass (2927.96 Da) matches well with the theoretical value (2927.63 Da, n = 25, with Ag^+), demonstrating the high efficient transformation of PS-N_3 into the PS-NH-COR in quantitative.

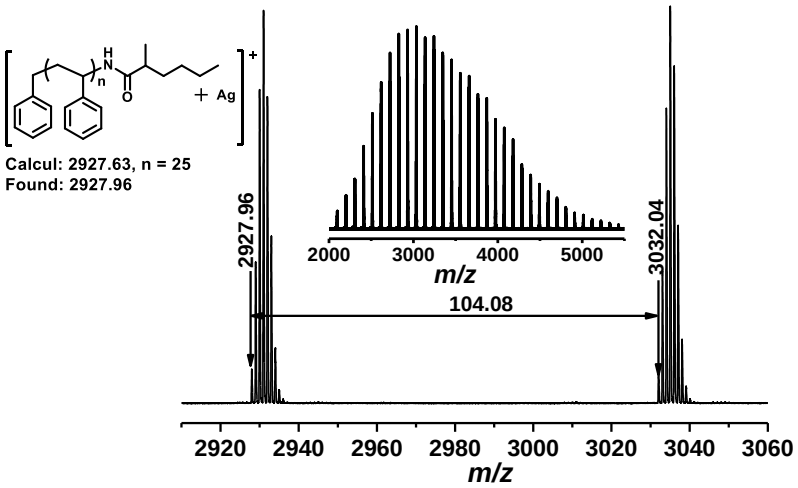

Fig. S37 MALDI-TOF-MS spectrum of the amide-functionalized PS via the catalytic S-V reaction of PS-N_3 with 2-methylhexanoic acid (Table 2, entry 6).

The acylation reaction of end group of PS-N_3 with pivalic acid

Fig. S38 shows the MALDI-TOF-MS spectrum of the end-functionalized PS via the catalytic S-V reaction of PS-N_3 with pivalic acid. Only a single polymer peak distribution is observed, and the experimental mass (2899.65 Da) matches well with the theoretical value (2899.53 Da, n = 25, with Ag^+), demonstrating the high efficient transformation of PS-N_3 into the PS-NH-COR in quantitative.

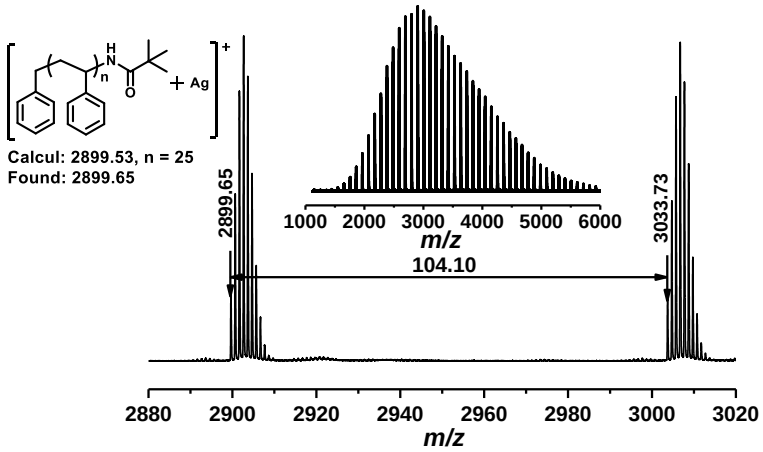

Fig. S38 MALDI-TOF-MS spectrum of the amide-functionalized PS via the catalytic S-V reaction of PS-N_3 with pivalic acid (Table 2, entry 7).

The acylation reaction of end group of PS-N_3 with Boc-Gly-OH

Fig. S39 shows the MALDI-TOF-MS spectrum of the end-functionalized PS via the catalytic S-V reaction of PS-N_3 with Boc-Gly-OH. As shown in Fig. S39, the end-functionalized PS exhibits five distinct distributions in the MALDI-TOF-MS spectrum, when analyzed using reflector mode detection. And all experimental mass match well with the theoretical value, except the peak at 2891.54 Da. The fragment ions (2891.54 Da) might represent distributions of the PS without azido functionality. [PS-$NHCOCH_2NH$+Ag]$^+$ and [PS-$NHCOCH_2$+Ag]$^+$ result from the cleavage of the amide bond of the end-functionalized PS. The remaining two fragment ions are PS-macromonomer (experimental mass = 2902.63 Da and theoretical value = 2902.50 Da, n = 26, with Ag^+) with an unsaturated C=C bond and [PS-N+Ag]$^+$ (experimental mass = 2917.93 Da and theoretical value = 2917.51 Da, n = 26, with Ag^+). Because the azide group of PS-N_3 was so weak that the bond could be cleaved to generate the fragments of PS-macromonomer and [PS-N+Ag]$^+$ during the MALDI-TOF-MS analysis. Therefore, it was not rigorous to characterize the efficiency of acylation reaction of PS-N_3 with Boc-Gly-OH only by MALDI-TOF-MS.

To further verify the efficiency of acylation reaction, both PS-N_3 and the end-functionalized PS were analyzed by ^{1}H NMR (Fig. S40). As shown in Fig. S40, the spectrum clearly shows the shift of the resonance for the proton next to the azide group from 3.93 ppm (PS-N_3) to 3.48 ppm (the end-functionalized PS), which also confirms successful transformation. According to the analysis results by MALDI-TOF-MS and ^{1}H NMR spectra (Fig.s S39 and S40), we confirmed that the chain-end functionality of PS was higher than 96%.

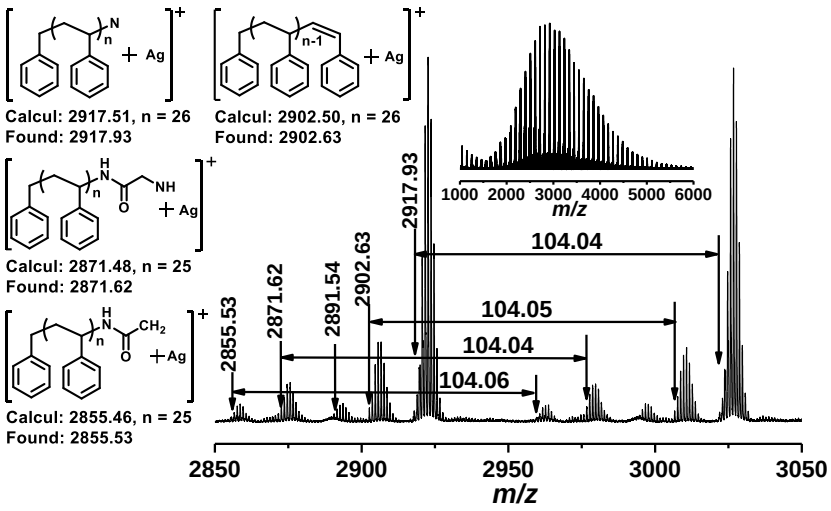

Fig. S39 MALDI-TOF-MS spectrum of the amide-functionalized PS via the catalytic S-V reaction of PS-N_3 with Boc-Gly-OH (Table 2, entry 8).

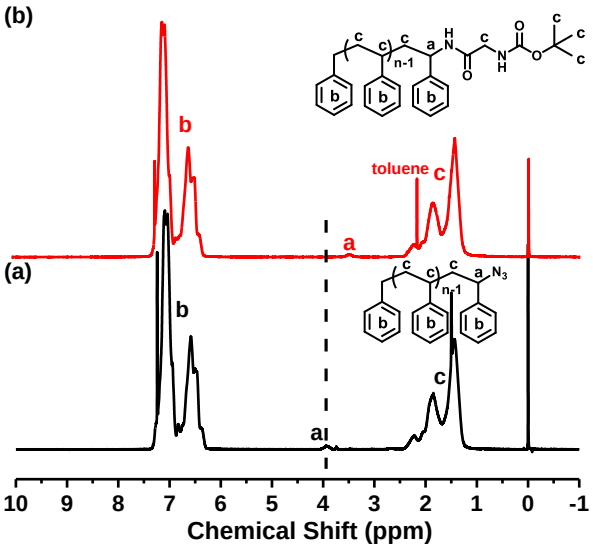

Fig. S40 ^{1}H NMR spectra of pre-prepared PS-N_3 (a) and the amide-functionalized PS (b) via the catalytic S-V reaction of PS-N_3 with Boc-Gly-OH (Table 2, entry 8) at 25 °C in $CDCl_3$.

The acylation reaction of end group of PS-N_3 with 1-naphthoic

Fig. S41 shows the MALDI-TOF-MS spectrum of the end-functionalized PS via the catalytic S-V reaction of PS-N_3 with 1-naphthoic. As shown in Fig. S41, the end-functionalized PS exhibits five distinct distributions in the MALDI-TOF-MS spectrum, when analyzed using reflector mode detection (Fig. S41). And all experimental mass match well with the theoretical value, except the tiny peak at 2751.33 Da. The two main fragment ions are $[PS\text{-}NHCOR+Ag]^+$ and $[PS\text{-}NHCOR+Na]^+$. The remaining two fragment ions are PS-macromonomer (experimental mass = 2902.53 Da and theoretical value = 2902.50 Da, n = 26, with Ag^+) with an unsaturated C=C bond and $[PS\text{-}NH+Ag]^+$ (experimental mass = 2918.58 Da and theoretical value = 2918.52 Da, n = 26, with Ag^+). The chain-end functionality of PS was higher than 98%, which was roughly estimated from the MALDI-TOF-MS spectrum with a 10% estimated error.

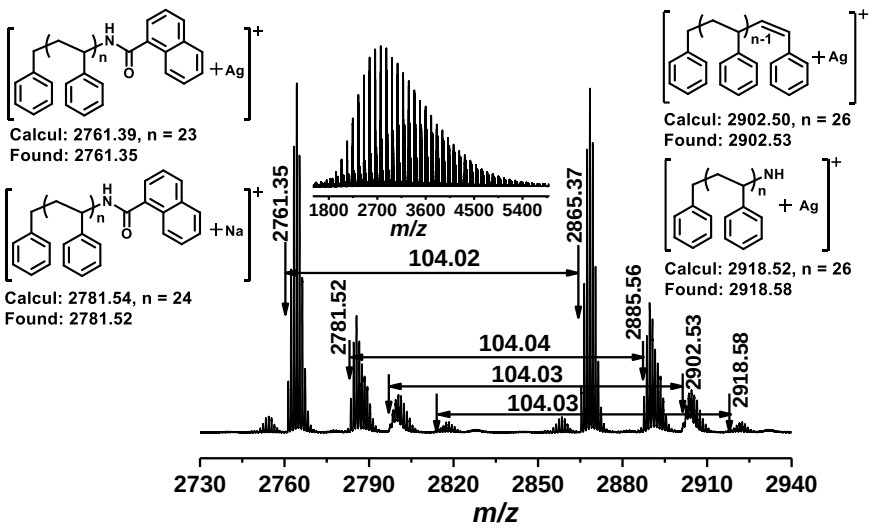

Fig. S41 MALDI-TOF-MS spectrum of the amide-functionalized PS via the catalytic S-V reaction of PS-N_3 with 1-naphthoic (Table 2, entry 9).

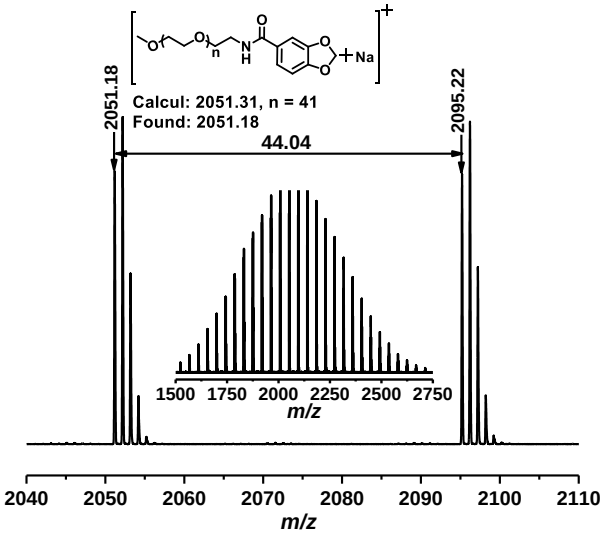

Fig. S42 MALDI-TOF-MS spectrum of the amide-functionalized PEG via the catalytic S-V reaction of PEG-N_3 with piperonylic acid (Table 2, entry 10).

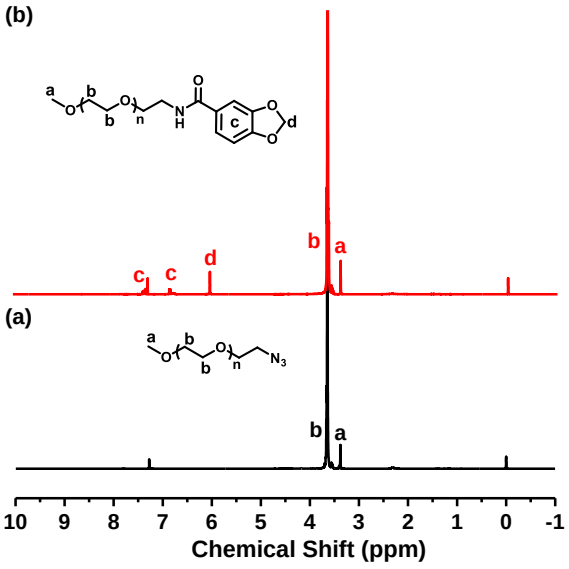

Fig. S43 (a) ^{1}H NMR spectra of pre-prepared PEG-N_3; (b) the amide-functionalized PEG obtained via the S-V reaction of PEG-N_3 with piperonylic acid (Table 2, entry 10) at 25 °C in $CDCl_3$.

The acylation reaction of end group of N_3-PS-N_3 with piperonylic acid

The efficiency of amidation reaction of N_3-PS-N_3 with piperonylic acid was evident in the MALDI-TOF-MS (Fig. S44). Only a single polymer peak distribution is observed and the experimental mass (3453.12 Da) matches well with the theoretical value (3452.79 Da, $n_1+n_2 = 28$, with Ag^+). In addition, ^1H NMR spectrum of the end amide-functionalized PS further confirmed the high efficiency of the end functionalization (Fig. S45). As shown in Fig. S45, the signal corresponding to the OCH_3 moiety is clearly observed (b, in Fig. S45), which indicates the introduction of the COR moiety on the chain-end of the polystyrene. The chain-end functionality of the product is estimated to be approximately 99% (with ±5% experimental error) from the relative peak areas of the two characteristic peaks (b and e in Fig. S45).

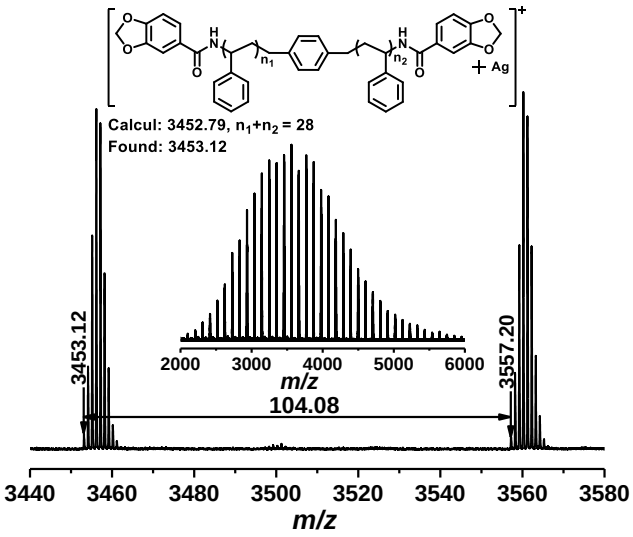

Fig. S44 MALDI-TOF-MS spectrum of the amide-functionalized PS via the catalytic S-V reaction of N_3-PS-N_3 with piperonylic acid (Table 2, entry 11).

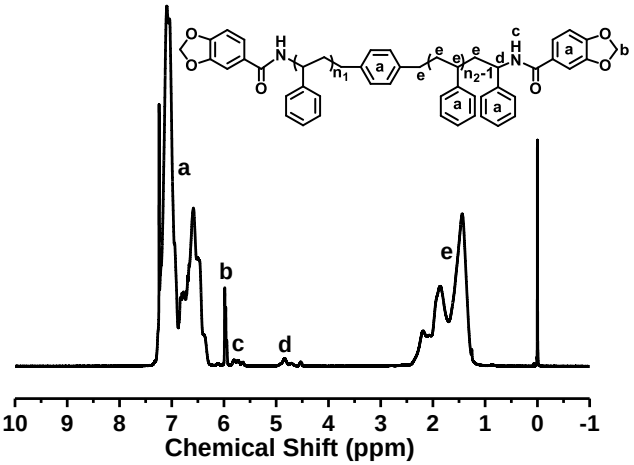

Fig. S45 ^1H NMR spectrum of the amide-functionalized PS via the catalytic S-V reaction of N_3-PS-N_3 with piperonylic acid (Table 2, entry 11) at 25 °C in $CDCl_3$.

The acylation reaction of end group of N_3-PS-N_3 with benzoic acid

Fig. S46 shows the MALDI-TOF-MS spectrum of the end-functionalized PS via the catalytic S-V reaction of N_3-PS-N_3 with benzoic acid. As shown in Fig. S46, the end-functionalized PS exhibits two distinct distributions in the MALDI-TOF-MS spectrum, when analyzed using reflector mode detection. And all experimental mass matches well with the theoretical value. One is fragment ions of target product ([ROCHN-PS-NHCOR+Ag]$^+$, experimental mass = 3052.51 Da and theoretical value = 3052.45 Da, $n_1+n_2 = 26$, with Ag^+). The other is fragment ions of [ROCHN-PS-macromonomer+Ag]$^+$ (experimental mass = 3035.57 Da and theoretical value = 3035.55 Da, $n_1+n_2 = 24$, with Ag^+)), which resulted from the cleavage of the amide bond of the end-functionalized PS. The chain-end functionality of PS is higher than 99%, which is roughly estimated from the MALDI-TOF-MS spectrum with a 10% estimated error.

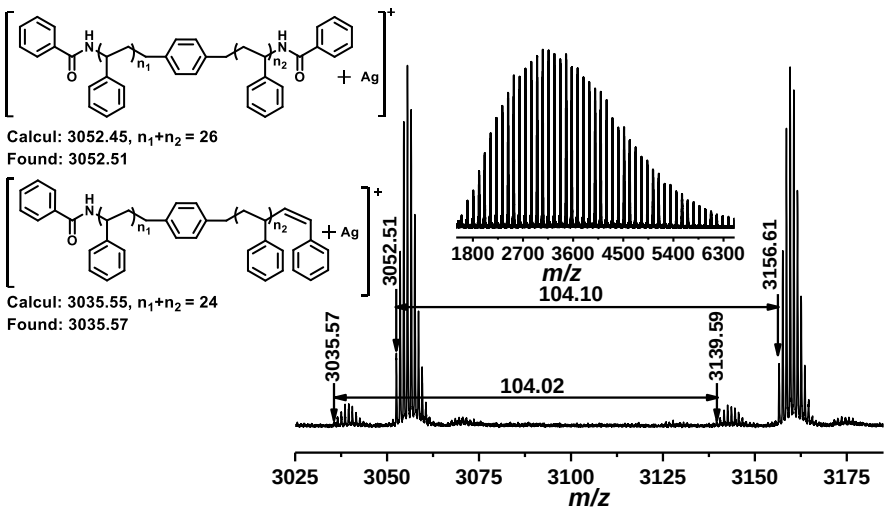

Fig. S46 MALDI-TOF-MS spectrum of the amide-functionalized PS via the catalytic S-V reaction of N_3-PS-N_3 with benzoic acid (Table 2, entry 12).

The acylation reaction of end group of N_3-PS-N_3 with stearic acid

Fig. S47shows the MALDI-TOF-MS spectrum of the end-functionalized PS via the catalytic S-V reaction of N_3-PS-N_3 with stearic acid. Only a single polymer peak distribution is observed, and the experimental mass (3065.36 Da) matches well with the theoretical value (3064.90 Da, $n_1+n_2 = 22$, with Ag^+), which indicates the high efficient transformation of N_3-PS-N_3 into the ROC-HN-PS-NH-COR in quantitative. The chain-end functionality of PS is higher than 99%, which is roughly estimated from the MALDI-TOF-MS spectrum with a 10% estimated error.

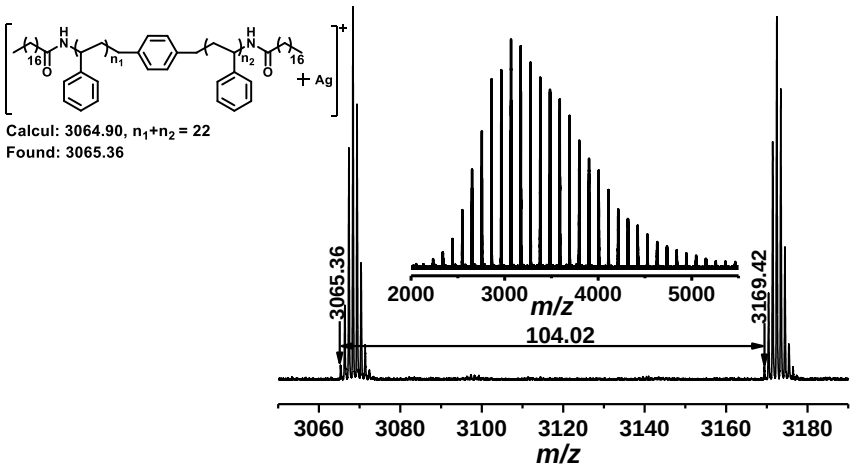

Fig. S47 MALDI-TOF-MS spectrum of the amide-functionalized PS via the catalytic S-V reaction of N_3-PS-N_3 with stearic acid (Table 2, entry 13).

The acylation reaction of end group of N_3-PS-N_3 with pivalic acid

Fig. S48 shows the MALDI-TOF-MS spectrum of the end-functionalized PS via the catalytic S-V reaction of N_3-PS-N_3 with pivalic acid. Only a single polymer peak distribution is observed, and the experimental mass (3429.36 Da) matches well with the theoretical value (3428.94 Da, $n_1+n_2 = 29$, with Ag^+), which indicates the high efficient transformation of N_3-PS-N_3 into the ROC-HN-PS-NH-COR in quantitative. The chain-end functionality of PS is approximately 100%, which is roughly estimated from the MALDI-TOF-MS spectrum with a 10% estimated error.

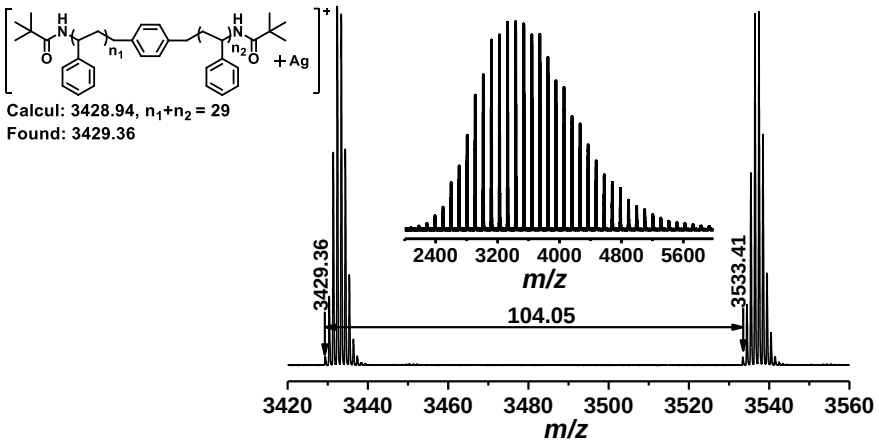

Fig. S48 MALDI-TOF-MS spectrum of the amide-functionalized PS via the catalytic S-V reaction of N_3-PS-N_3 with pivalic acid (Table 2, entry 14).

2. The Coupling Reaction between Polymer-N_3 and Multifunctional Coupling Agent

Scheme 7 Schematic Representation of Construction of Amide-Functionalized (Multi)block, Star Polymers via the Catalytic S-V Reaction

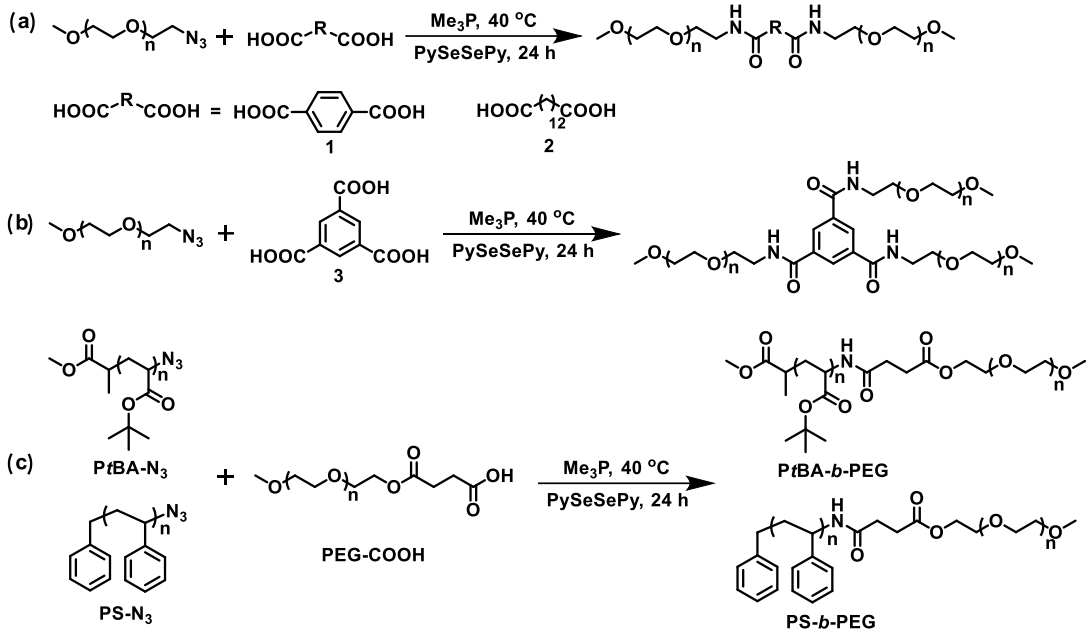

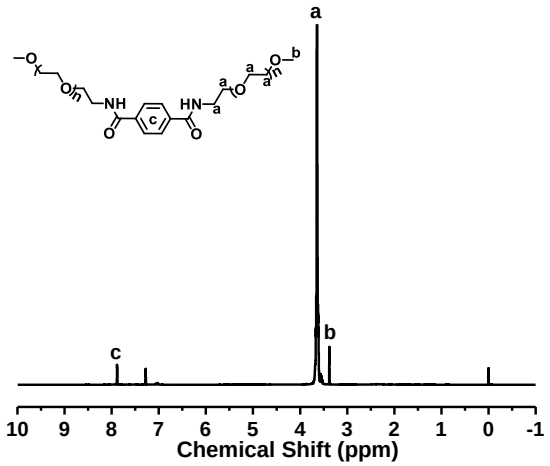

Fig. S49 ^{1}H NMR spectrum of the product of the coupling reaction between PEG-N_3 and terephthalic acid (PEG-PEG) at 25 °C in $CDCl_3$.

Scheme S8 The synthetic route of amide-functionalized block polymers via thecatalytic S-V reaction of PEG-N_3 with tetradecanedioic acid

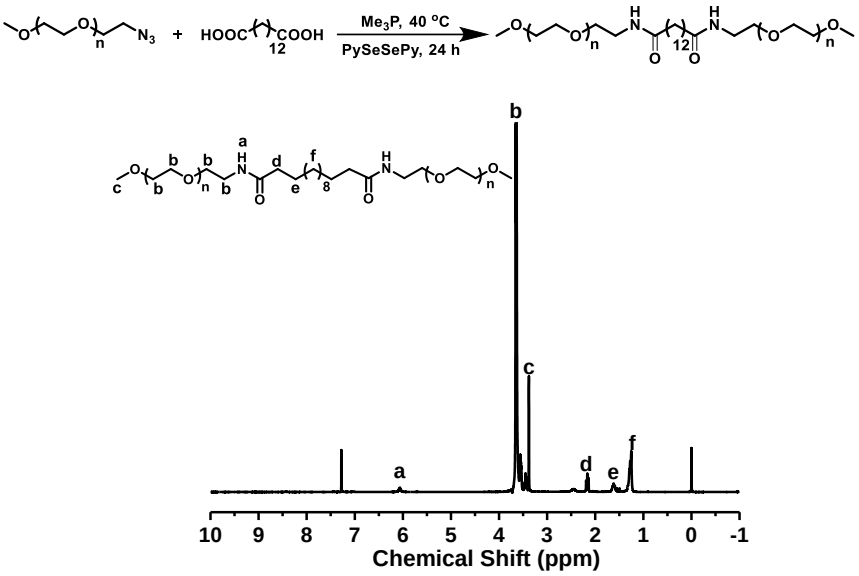

Fig. S50 ^{1}H NMR spectrum of the coupling product of pre-prepared PEG-N_3 with tetradecanedioic acid (PEG-PEG) at 25 °C in $CDCl_3$.

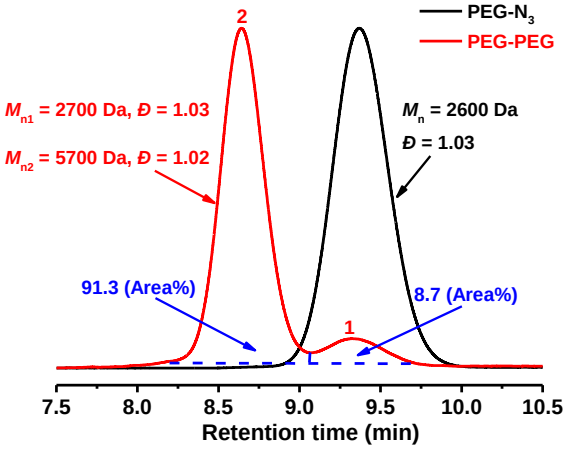

Fig. S51 SEC curves of pre-prepared PEG-N_3 and its coupling product with tetradecanedioic acid (PEG-PEG). THF was used as the eluent and PS standards as the calibration.

The efficiency of the catalytic S-V potential click coupling reaction of PEG-N_3 with tetradecanedioic acid was characterized by ^{1}H NMR and SEC (Fig.s S50 and S51). The ^{1}H NMR spectra of pre-prepared PEG-N_3 and the coupling product with tetradecanedioic acid were respectively shown in Fig.s S43a and S50. The new resonance signal at 6.06 ppm (a, Fig. S50) in ^{1}H NMR spectrum is attributed to the amide proton, which indicates the successful coupling of PEG-N_3. And the percentage of the coupling product (PEG-PEG) is up to 95% (with ±5% experimental error), which is estimated from the protons of methoxy group (c, in Fig. S50) and the relative peak areas of characteristic peak (methylene protons, d, in Fig. S50). Furthermore, the estimated result by ^{1}H NMR is in good accordance with the peak splitting result of the SEC curve of the PEG-PEG coupling product using Gaussian function (Fig. S51).[11] After the coupling reaction, there are two peak distributions in the SEC curve (red, Fig. S51). And the area fraction of the coupling polymer (PEG-PEG) is about 91.3% in the SEC curve. The rest of the PEG chains, with 8.7% area fraction, were expected to be a mixture of PEG chains containing a mono-amido group at the one chain end and PEG without azido functionalization.

Scheme S9 The synthetic route of amide-functionalized block polymers via the catalytic S-V reaction of PS-N_3 with terephthalic acid

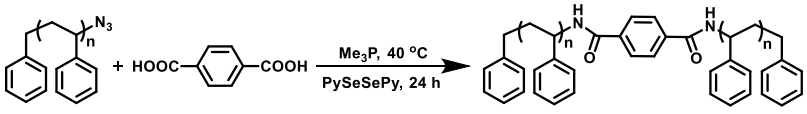

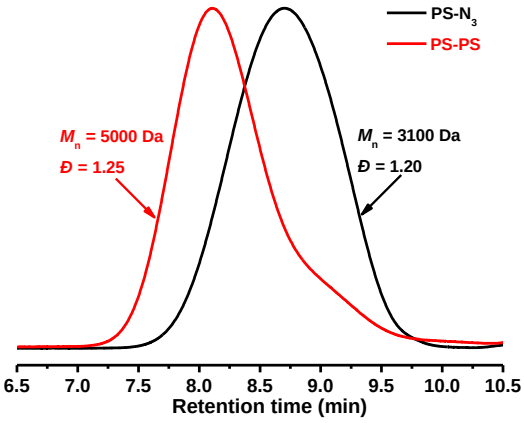

Fig. S52 SEC curves of pre-prepared PS-N_3 and its coupling product with terephthalic acid (PS-PS). THF was used as the eluent and PS standards as the calibration.

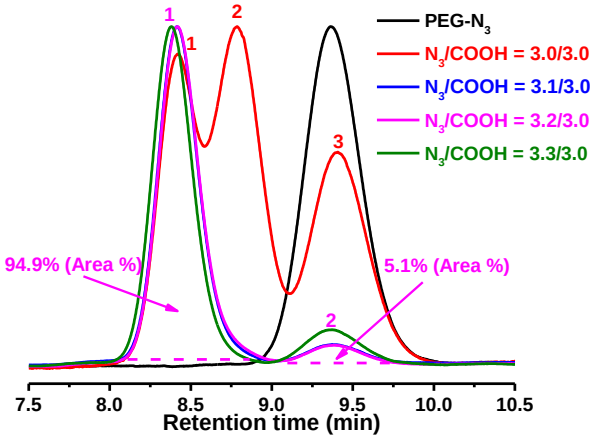

Fig. S53 SEC curves of pre-prepared PEG-N_3 and its coupling product with trimesic acid. THF was used as the eluent and PS standards as the calibration.

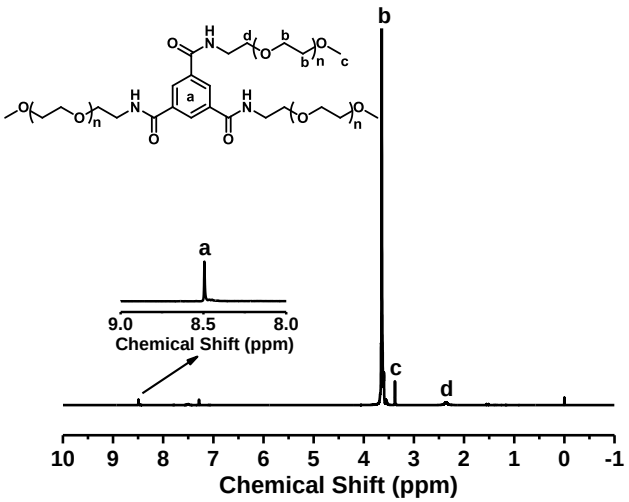

Fig. S54 ^{1}H NMR spectrum of the coupling product (3-arm star PEG) of pre-prepared PEG-N_3 with trimesic acid (Table 3, entry 4) at 25 °C in $CDCl_3$.

Scheme S10 The synthetic route of amide-functionalized 3-arm Star polymers via the catalytic S-V reaction of PS-N_3 with trimesic acid.

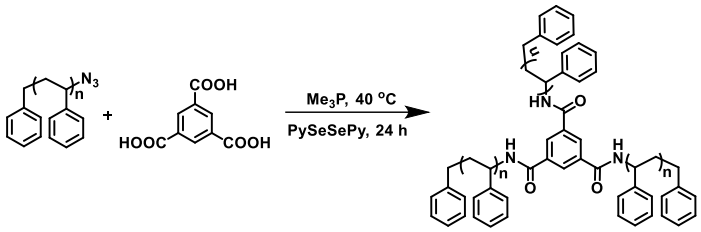

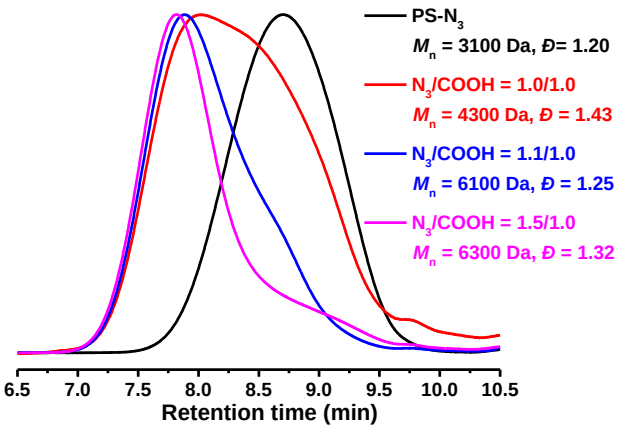

Fig. S55 SEC curves of pre-prepared PS-N_3 and its coupling product with trimesic acid. THF was used as the eluent and PS standards as the calibration.

As shown in Fig. S55, the product of the 3-arm star PS contained some of the double coupling product (PS-PS) when the 3-arm star polymer was prepared through the catalytic S-V reaction of PS-N_3 with trimesic acid (coupling agent **3**), which was possibly owing to the large steric bulk of PS-N_3.

3. Synthesis of block polymers

1) Synthesis and Characterization of P*t*BA-N_3 and PEG-COOH

Scheme S11 Schematic Illustration of Synthesis of P*t*BA-N_3.

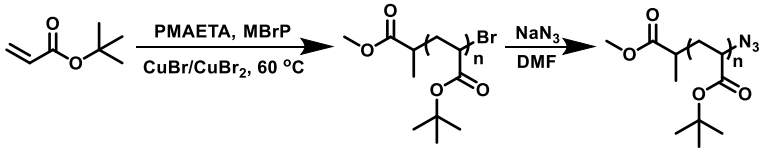

Synthesis of P*t*BA-N_3. In a dry 50 mL Schlenk flask CuBr (0.3175 g, 2.2130 mmol), copper (II) bromide ($CuBr_2$) (0.0247 g, 0.1106 mmol), PMDETA (0.4026 g, 2.323 mmol), methyl 2-bromopropionate (0.7391 g, 4.426 mmol) were mixed together. Then *t*-BA (18.88 g, 147.3 mmol) and dimethyl sulfoxide (20 mL) were injected into the mixture, followed sealing with a rubber bung. The mixture was degassed by three consecutive freeze-pump-thaw cycles and was placed into an oil bath at 60 °C with stirring. After 3 h, the reaction was stopped and the flask was allowed to cool to room temperature. Then the mixture was dissolved in THF and copper salts were removed through a neutral alumina column. The filtrate was precipitated in a water/methanol (v/v = 1/1) mixture solvent. The polymer was obtained by filtration and dried in a vacuum oven at 60 °C for 24 h (P*t*BA-Br, 11.5 g, yield: 59%, M_n = 5000 Da, $Đ$ = 1.17).

P*t*BA-Br (6.0 g, 1.2 mmol), NaN_3 (1.560 g, 24 mmol) and DMF (35 mL) were added into a 100 mL round-bottom flask. Then the mixture was reacted in an oil bath at 60 °C with a magnetic stirring for 24 h. After cooling to room temperature, the mixture was passed through a neutral alumina column to remove residual sodium salts. Then the solution was precipitated in a water/methanol (v/v = 1/1) mixture solvent. The polymer was obtained by filtration and dried in a vacuum oven at 60 °C for 24 h (P*t*BA-N_3, 4.16 g, yield: 69%, M_n = 5200 Da, $Đ$ = 1.15).

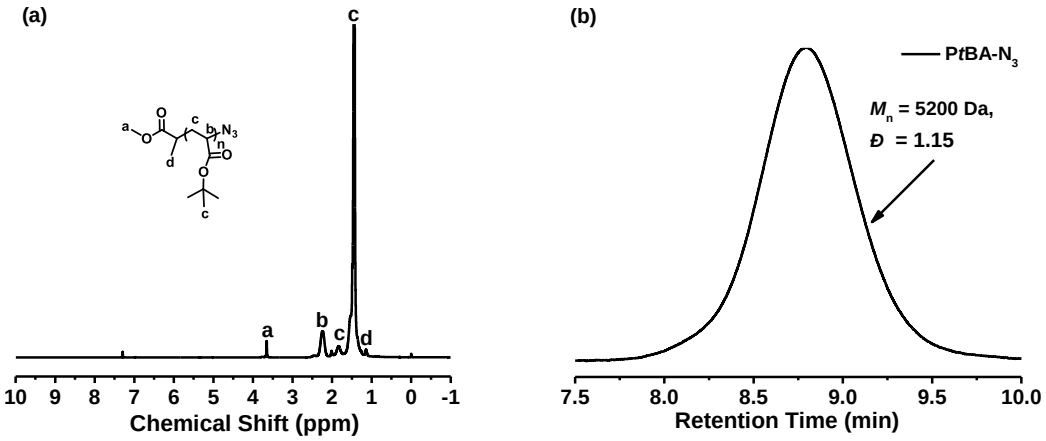

Fig. S56 (a) ^{1}H NMR spectrum of P*t*BA-N_3 at 25 °C in $CDCl_3$; (b) SEC curve of P*t*BA-N_3. THF was used as the eluent and PMMA standards as the calibration.

Scheme S12 Schematic Illustration of Synthesis of PEG-COOH.

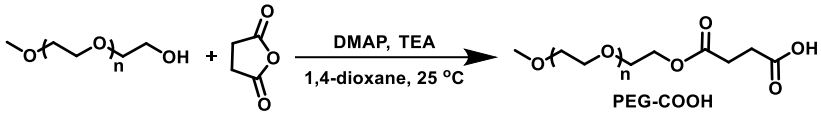

Synthesis of PEG-COOH. PEG-OH (10.0 g, 5.263 mmol), succinic anhydride (0.7900 g, 7.895 mmol), 4-dimethylaminopyridine (0.9645 g, 7.895 mmol), trimethylamine (0.7989 g, 7.895 mmol) and 1,4-dioxane (400 mL) were added into a 500ml three-necked round-bottom flask equipped with nitrogen atmosphere and magnetic stirrer. The reaction mixture was stirred at 25 °C for 24 h. Then the mixture was filtered to remove salts and 1,4-dioxane was removed under vacuum. The filtered solution was precipitated into an excess of cold diethyl ether. After re-precipitation into cold diethyl ether, the product was dried under vacuum for 12 h (PEG-COOH, 9.0 g, yield: 90%, M_n = 2200 Da, $Đ$ = 1.07).

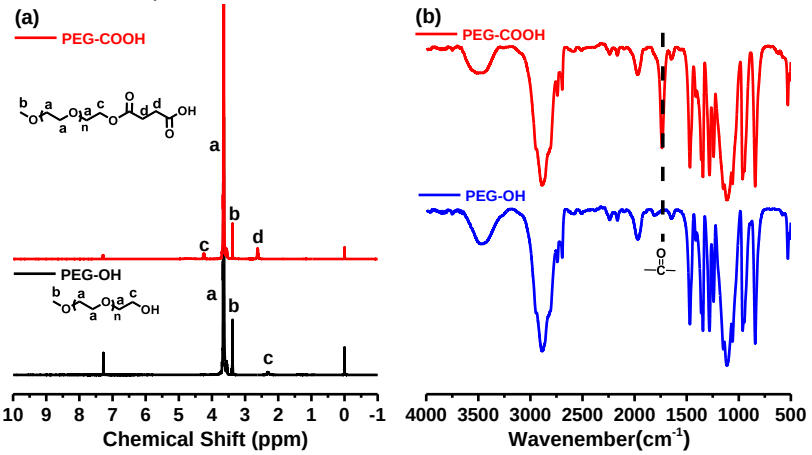

Fig. S57 (a) ^{1}H NMR spectra of PEG-COOH and PEG-OH at 25 °C in $CDCl_3$; (b) FT-IR spectra of PEG-COOH and PEG-OH.

As shown in Fig. S57a, the spectra clearly show the shift of the resonance for the proton next to the hydroxy end group from 2.38-2.18 ppm (PEG-OH) to 4.27-4.22 ppm (PEG-COOH), which confirms successful synthesis of PEG-COOH. And the characteristic absorption bands of C=O group appears at 1745 cm^{-1} in FT-IR spectrum (red, Fig. S57b), which further indicates the successful synthesis of PEG-COOH. As shown in Fig. S58, PEG-COOH exhibits two distinct distributions in the MALDI-TOF-MS spectrum when analyzed using reflector mode detection. The fragment ions of $[PEG\text{-}COOH+H]^+$ (experimental mass = 2114.28 Da and theoretical value = 2114.39 Da, n = 44) are observed in the MALDI-TOF-MS spectrum. The other is fragment ions of $[PEG\text{-}COOH+Na]^+$ (experimental mass = 2136.35 Da and theoretical value = 2136.38 Da, n = 44). In addition, no other indeterminate polymer peak distribution was observed in the MALDI-TOF-MS spectrum, indicating that the PEG-COOH was the only product.

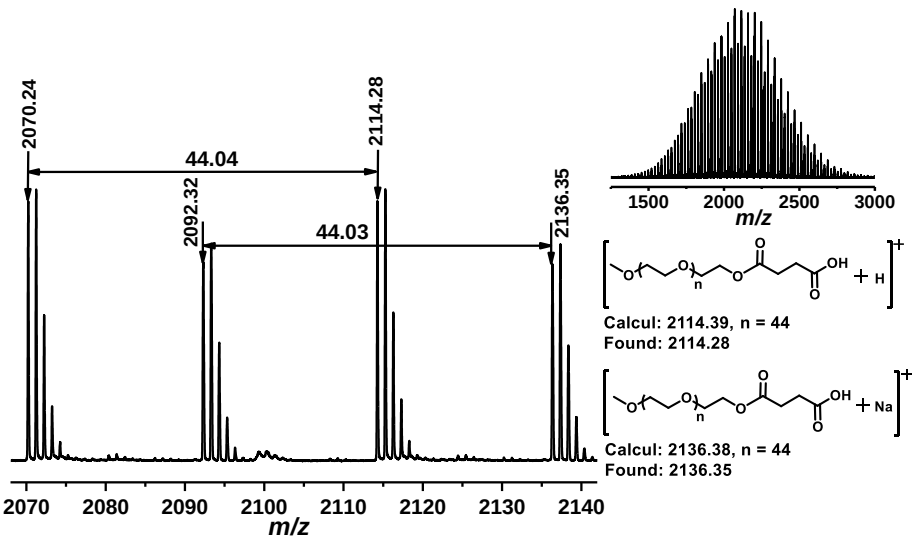

Fig. S58 MALDI-TOF-MS spectrum of PEG-COOH obtained via the reaction of PEG-OH with SA.

2) Results and Discussion

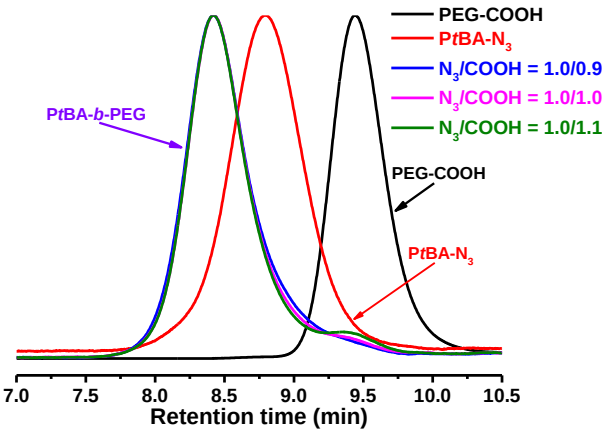

Fig. S59 SEC curves of PEG-COOH, P*t*BA-N_3 and P*t*BA-*b*-PEG. THF was used as the eluent and PMMA standards were used for the calibration.

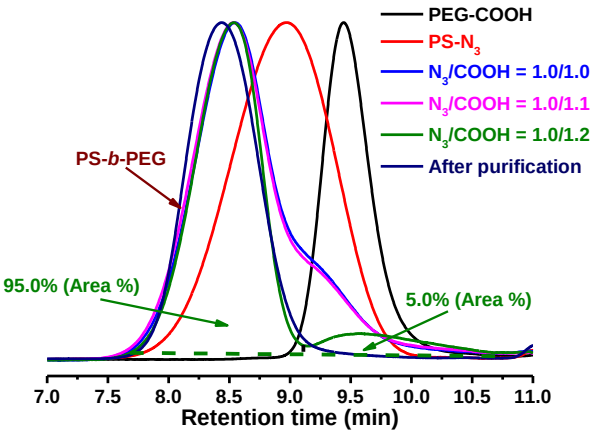

Fig. S60 SEC curves of PEG-COOH, PS-N_3 and PS-*b*-PEG. THF was used as the eluent and PS standards were used for the calibration.

4. The Preparation of Amide-Functionalized Side Chain Polymers

Scheme S13. The Synthesis and Post-Polymerization Modification of P(S-*co*-CMS-N_3).

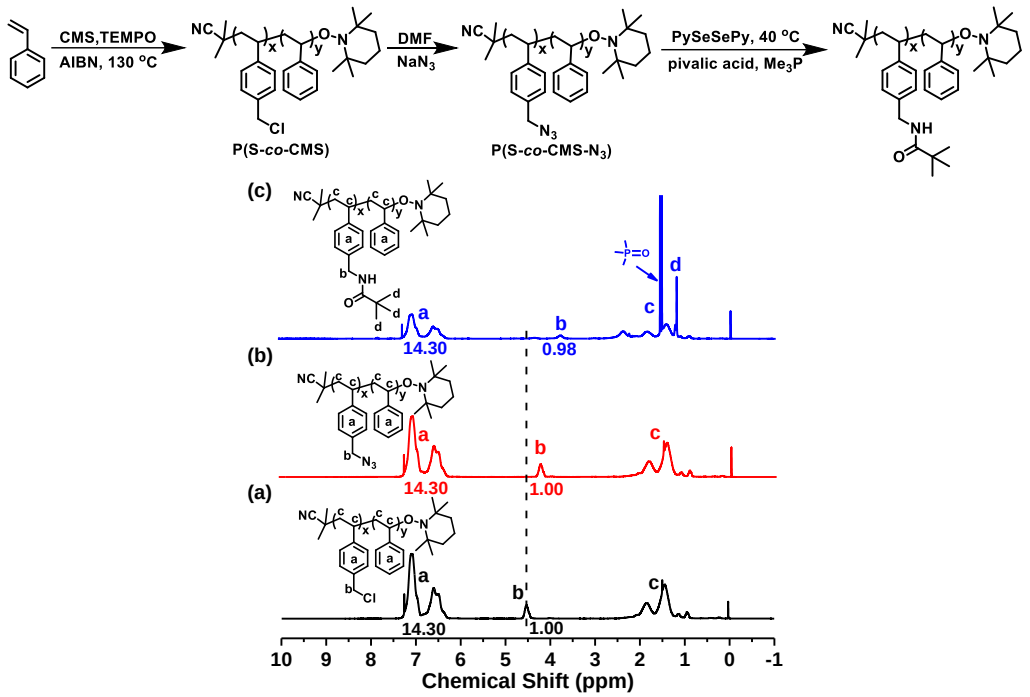

Fig. S61 ^{1}H NMR spectra of the side-chain amide-functionalized PS (c), pre-prepared P(S-*co*-CMS-N_3) (b) and P(S-*co*-CMS) (a) at 25 °C in $CDCl_3$.

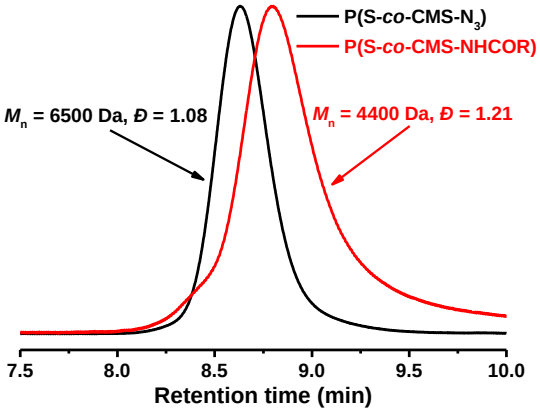

Fig. S62 SEC curves of the side-chain amide-functionalized PS (red), pre-prepared P(S-*co*-CMS-N_3) (black). DMF was used as the eluent and PS standards were used for the calibration.

Section C. References

1. K. Bhasin and J. Singh, *J. Organomet. Chem.*, 2002, **658**, 71-76.
2. J. R. Thomas, X. Liu and P. J. Hergenrother, *J. Am. Chem. Soc.*, 2005, **127**, 12434-12435.
3. Y. X. Lei, H. Li, W. X. Gao, M. C. Liu, J. X. Chen, J. C. Ding, X. B. Huang and H. Y. Wu, *J. Mater. Chem. C*, 2014, **2**, 7402-7410.
4. C. A. Anderson, P. G. Taylor, M. A. Zeller and S. C. Zimmerman, *J. Org. Chem.*, 2010, **75**, 4848-4851.
5. C. Bakkali-Hassani, D. Tunc, K. Roos, M. Planes, P. Lecomte and S. Carlotti, *Macromolecules*, 2016, **50**, 175-181.
6. L. Jasinska, M. Villani, J. Wu, D. van Es, E. Klop, S. Rastogi and C. E. Koning, *Macromolecules*, 2011, **44**, 3458-3466.
7. (a) G. P. Kar, P. Xavier and S. Bose, *Phys. Chem. Chem. Phys.*, 2014, **16**, 17811-17821; (b) K. Matyjaszewski, Y. Nakagawa and S. G. Gaynor, *Macromol. Rapid Commun.*, 1997, **18**, 1057-1066; (c) K. Susumu, B. C. Mei and H. Mattoussi, *Nat. Protoc.*, 2009, **4**, 424-436.
8. (a) M. Lansalot, C. Farcet, B. Charleux, J. P. Vairon and R. Pirri, *Macromolecules*, 1999, **32**, 7354-7360; (b) C. Ladaviere, P. Lacroix-Desmazes and F. Delolme, *Macromolecules*, 2008, **42**, 70-84; (c) L. Charles, *Mass Spec. Rev.*, 2014, **33**, 523-543.
9. Y. Li, J. N. Hoskins, S. G. Sreerama and S. M. Grayson, *Macromolecules*, 2010, **43**, 6225-6228.
10. C. Chen, L. Q. Xiao and A. Goto, *Macromolecules*, 2016, **49**, 9425-9440.
11. H. Gao and K. Matyjaszewski, *Macromolecules*, 2006, **39**, 4960-4965.